Mon. Not. R. Astron. Soc. **000**, 000–000 (0000) Printed 21 August 1997 (MN LaTeX style file v1.4)

THE ORIGIN OF THE COSMIC SOFT X-RAY BACKGROUND: OPTICAL IDENTIFICATION OF AN EXTREMELY DEEP ROSAT SURVEY

I M M^c Hardy[1], L R Jones[1,2], M R Merrifield[1], K O Mason[3], A M Newsam[1], R G Abraham[4,5], G B Dalton[7], F Carrera[3,6], P J Smith[3], M Rowan-Robinson[8], G A Wegner[9], T J Ponman[2], H J Lehto[10], G Branduardi-Raymont[3], G A Luppino[11], G Efstathiou[7], D J Allan[2], J J Quenby[8].

[1] *Department of Physics and Astronomy, The University, Southampton SO17 1BJ*
[2] *School of Physics and Space Research, University of Birmingham, Edgbaston, Birmingham B15 2TT.*
[3] *Mullard Space Science Laboratory, University College London, Holmbury St Mary, Dorking RH5 6NT*
[4] *Dominion Astrophysical Observatory, 5071 West Saanich Road, Victoria V8X 4M6, British Columbia, Canada.*
[5] *Institute of Astronomy, Madingley Road, Cambridge CB3 0HA.*
[6] *Instituto de Fisica de Cantabria, 39005 Santander, Spain.*
[7] *Department of Astrophysics, Keble Road, Oxford OX1 3RH.*
[8] *Department of Physics, Imperial College, Prince Consort Road, London SW7 2BZ.*
[9] *Department of Physics and Astronomy, Dartmouth College, Hanover, NH 03755, USA.*
[10] *Tuorla Observatory, Turku University, Piikkiö, FIN-21500, Finland.*
[11] *University of Hawaii, Institute for Astronomy, 2680 Woodlawn Drive, Honolulu, Hawaii 96822, USA.*

21 August 1997

ABSTRACT

We present the results of the deepest optically identified X-ray survey yet made. The X-ray survey was made with the ROSAT PSPC and reaches a flux limit of 1.6×10^{-15} erg cm^{-2} s^{-1} (0.5 -2.0 keV). Above a flux limit of 2×10^{-15} erg cm^{-2} s^{-1} we define a complete sample of 70 sources of which 59 are identified. For a further 5 sources we have tentative identifications and for a further 4 the X-ray error-boxes are blank to R=23 mag. At brighter fluxes ($\geq 10^{-14}$ erg cm^{-2} s^{-1}) we confirm the results of previous less deep X-ray surveys with 84% of our sources being QSOs. However at the faint flux limit the survey is dominated by a population of galaxies with narrow emission lines (NELGs). In addition at intermediate fluxes we find a small number of groups and clusters of galaxies at redshifts generally > 0.3. Most of these groups are poor systems of low X-ray luminosity and the number which we find is consistent with a zero evolutionary scenario, unlike the situation for high luminosity clusters at the same redshift. To a flux limit of 2×10^{-15} erg cm^{-2} s^{-1} QSOs contribute $> 31\%$ of the cosmic soft X-ray background (XRB), groups/clusters contribute $\sim 10\%$ and NELGs contribute $\sim 8\%$. However the QSO differential source count slope below 10^{-14} erg cm^{-2} s^{-1} is $\sim$-1.4, severely sub-Euclidean, as is the (poorly defined) group/cluster slope, whereas the differential NELG slope is close to Euclidean (~ -2.4). If the NELG source counts continue to rise at that slope, all of the remaining cosmic soft XRB will be explained by a flux limit of $\sim 1-2\times10^{-16}$ erg cm^{-2} s^{-1} with NELGs contributing about one quarter of the XRB. The average NELG X-ray spectrum is harder than that of the QSOs, and similar to that of the remaining unresolved cosmic (XRB) suggesting that NELGs will also be substantial contributors to the XRB at higher energies. The observed NELGs lie in the redshift range 0.1-0.6 and have $M_R = -20$ to -23, approximately 3 magnitudes more luminous than typical field galaxies. They have predominantly blue colours, and some are definitely spirals, but the presence of some ellipticals cannot yet be ruled out. Many are in interacting or disturbed systems. The NELGs have optical spectra similar to those of the majority of the field galaxy population at a similar redshift and may simply be the more luminous members of the emission line field galaxy population. Based on optical line ratios and X-ray/optical ratios, the NELGs, both as a sample and within individual galaxies, appear to be a mixture of starburst galaxies and true AGN.

Key words: X-ray background, emission line galaxies, QSOs, clusters of galaxies.

1 INTRODUCTION

The origin of the extragalactic X-ray background (XRB) is one of the key questions in astrophysics. The excellent fit of the microwave background, as observed by COBE, to a pure blackbody undistorted by Compton scattering from hot electrons, has ruled out a major contribution to the XRB ($\geq$few %) from diffuse hot gas (Mather *et al.* 1990), so a large collection of discrete sources must be responsible. Previous X-ray surveys with ROSAT have been dominated by QSOs (Shanks *et al.* 1991; Boyle *et al.* 1993) which, to a flux limit of 2×10^{-14} erg cm^{-2} s^{-1} (the band 0.5-2.0 keV is used throughout this paper), can account directly for >30% of the cosmic soft XRB. Here, following preliminary reports by Jones *et al.* (1995) and M^{c}Hardy (1995) which listed most of the major conclusions, we present full details of the deepest optically identified X-ray survey yet made which clarify the origin of the remainder of the cosmic soft XRB.

The X-ray data consist of a 115 ksec ROSAT PSPC observation reaching a flux limit of 1.6×10^{-15} erg cm^{-2} s^{-1} (Section 2). This observation was made in two parts and source counts from the first 73 ksec of the observation have already been given by Branduardi-Raymont *et al.* (1994 - hereafter GBR). Deep optical CCD images (Section 3.1) have been taken in V and R of the inner 15 arcmin radius of the ROSAT field to provide optical identifications and colours. Optical spectra (Section 3.2) have subsequently been taken of sources in a statistically complete sub-section comprising $\sim$ 80% of the 15 arcmin radius survey area. Deep radio surveys at 20 and 6 cm have also been made of the survey area and some preliminary results are presented here.

The main purpose of this paper is not to recalculate the integral source counts of GBR using an increased dataset, although we do present such counts, but to discuss the identification content of the survey (Section 4) and to consider the implications for the origin of the soft X-ray background. Within a region comprising $\sim$ 80% of the full 15 arcmin radius X-ray survey region, we have optical spectroscopic observations of almost all likely optical identifications for almost all X-ray sources. We refer to this regions as our (spectroscopically) 'complete area' and all discussion of the identification content of our survey refers to this area. We show that although QSOs dominate at the brighter flux levels, as found in previous ROSAT surveys, galaxies mainly with narrow emission lines (NELGs) dominate at the faintest flux levels. We also note that a small number of sources are definitely identified with groups or clusters of galaxies. The X-ray spectra of the various classes of identifications are discussed in Section 5 where they are compared with the spectrum of the remaining unresolved XRB. In Section 6 we calculate the contribution of the various classes of identified sources to the soft XRB and show that, if the NELG source counts extrapolate to $1 - 2 \times 10^{-16}$ erg cm^{-2} s^{-1} they will account for almost all of the remaining soft XRB. We also discuss their possible contribution to the XRB at higher energies. The optical spectra of the NELGs are compared with those of other narrow emission line galaxies such as starburst or Seyfert 2 galaxies in Section 7 and in Section 8 we compare the NELGs with field galaxies in a similar redshift range. In Section 9 we summarise our results.

2 ROSAT OBSERVATIONS

Observations with the ROSAT position sensitive proportional counter (PSPC) were made at position RA 13 34 37.0 Dec +37 54 44 (J2000), in a region of sky of extremely low obscuration ($N_H \sim 6.5 \times 10^{19}$ cm^{-2}). The low obscuration was initially found in the neutral hydrogen survey of Stark *et al.* (1992) and confirmed by analysis of the IRAS 100μ cirrus maps which showed very low emission in the chosen direction. The observations were made in two parts. The source counts resulting from the first 73 ksec observation in June 1991 have already been reported by GBR who provide details of the absorption measurements. Fluctuation analysis of these same data were presented by Barcons *et al.* (1994). These two initial papers show that the source density flattens off below a Euclidean distribution at fluxes less than 1.6×10^{-14} erg cm^{-2} s^{-1}.

A further observation of 42ksec was made with the PSPC in June and July 1993. Together these two observations comprise the second deepest ROSAT X-ray survey made. The deepest PSPC survey, of ~150ksec duration, is in the direction of the first Lockman hole (10h 48m +57°) by Hasinger *et al.* (1993) but optical results have not yet been published from that survey.

2.1 Source Searching

Initial analysis of the combined AO1 and AO4 data were carried out using the UK ASTERIX software system to create an image from the combined datasets. Following GBR we have rejected data with high anticoincidence rate (Master Veto Rate > 170) or bad aspect ratio. This has left 115ksec of 'clean' data. To optimise the search for point sources we have restricted the energy band to 0.5-2.0 keV. Below 0.5 keV there is a substantial contribution to the background from diffuse emission in our own galaxy and above 2.0 keV the particle background dominates. Source searching was carried out using our own software, based on the Cash (1979) statistic, including the radial variation of the psf. Our algorithm is essentially the same as the standard Starlink PSS source detection algorithm but improves the fitting of the local background. We set our detection criterion such that ~one of the sources in our survey is expected to be false. This is approximately the same as using a 3.5σ significance detection threshold.

Flux variability between the AO1 and AO4 observations is small with only ~20% of the sources showing variability, with a maximum detected variation of ~20% amplitude. We leave discussion of source variability to a future paper and here consider time-averaged fluxes.

To convert between count rate and flux we follow GBR and assume that the X-ray spectra of most sources are described by power laws of energy index α=+1.1 (where the flux, S, at an energy, E, is given by $S(E) \propto E^{-\alpha}$) and that the absorbing column is 6.5×10^{19} cm^{-2}. The conversion then is that 1 pspc (0.5-2.0 keV) count s^{-1} = 1.14×10^{-11} erg cm^{-2} s^{-1}. Varying the assumed column by 20% (eg to 8×10^{19} cm^{-2}) has no measureable effect on the conversion but varying α has a small effect. For example, assuming α=0.5 gives 1 pspc (0.5-2.0 keV) count s^{-1} = 1.18×10^{-11} erg cm^{-2} s^{-1}. In section 5 we will see that, although an energy index of ~ 1 is correct for the QSOs which comprise the majority of the bright sources, there is a population of faint galaxies with flatter spectra, $\alpha \sim 0.5$. However as the uncertainty in the count/flux conversion is a very small effect, particularly for faint sources where photon counting errors are noticeably larger, we continue to use the conversion factor appropriate to α= 1.1 for all sources.

2.2 Simulations

2.2.1 Completeness of the Survey

We have conducted simulations to determine the level of completeness of our survey and the accuracy of our positions. The simulations were carried out in a manner similar to that described in GBR. Each simulated observation consists of a single square frame 34 arcmin along each side with 4 arcsec square pixels. Sources are positioned randomly about the frame and assigned a flux between 2.0×10^{-16} and 5.0×10^{-14} erg cm^{-2} sec^{-1} drawn from the observed source counts of the survey with a linear extrapolation below 2.0×10^{-15} erg cm^{-2} sec^{-1}. We simulated 150 frames giving a total area of ~ 250 times that of the present deep survey.

The source detection algorithm is then applied to the simulated observation frame. In the simulations we use only the on-axis PSPC PSF throughout. The (small) effect of the radial variation of the psf and the effective area are considered below. The source fitting procedure produces a list of positions of 'found' sources ($x_f \pm \sigma_x, y_f \pm \sigma_y$) with measured fluxes ($F_f$). The observed positions and fluxes are then compared with the list of known 'real' (ie input) positions (x_r, y_r) and fluxes (F_r) in order to find likely matches. The comparison was performed as follows. Each 'real' source brighter than 1.0×10^{-15} erg cm^{-2} sec^{-1} is read in and compared to each of the 'found' sources within a 1 arcmin radius using a χ^2-like statistic:

$$S = \left(\frac{x_f - x_r}{\sigma_x}\right)^2 + \left(\frac{y_f - y_r}{\sigma_y}\right)^2 + \left(\frac{F_f - F_r}{\sqrt{F_r}}\right)^2 \qquad (1)$$

Each 'real' source is then matched with the best-fit (minimum-S) 'found' source and the resulting real/found pairs are removed from their respective source lists. The matching process continues until only unmatched 'real' and 'found' sources remain. Unmatched 'real' sources are referred to as missing sources and unmatched 'found' sources are referred to as spurious sources. In order to avoid edge-effects, all 'real' and 'found' sources within 1 arcmin of the edge of the simulated frames are removed from the analysis.

The statistic 'S' is distributed very much like the χ^2 statistic, ie the large majority of matches have a low value of S corresponding to 'real' and 'found' sources of very similar flux and position. A very small number of matches have large values of S, but that is just what we would expect in any real observation. We therefore do not impose any upper limit on the accepted value of S. Our only cut-offs are that the matches should occur within 1 arcmin and that we do not match 'real' sources of flux less than 1.0×10^{-15} erg cm^{-2} sec^{-1}. We could easily impose an upper cut-off on S, such as the equivalent of a 5σ confidence limit, but it would have a negligible effect on the number of matched sources.

The completeness of our survey is shown in figure 1. Here we plot the percentage of missed and spurious sources

Table 1. SURVEY COMPLETENESS: Missed and Spurious Sources in the 'Complete Area'

Measured Flux ($\times 10^{-15}$ erg cm^{-2} s^{-1})	2.00-2.49	2.50-3.14	3.15-4.09	4.10-5.99	6.0-9.99	10.0-17.4
Missed sources	1.6	1.8	2.0	0.8	0.6	0.3
Spurious sources	1.4	0.4	0.2	0	0	0

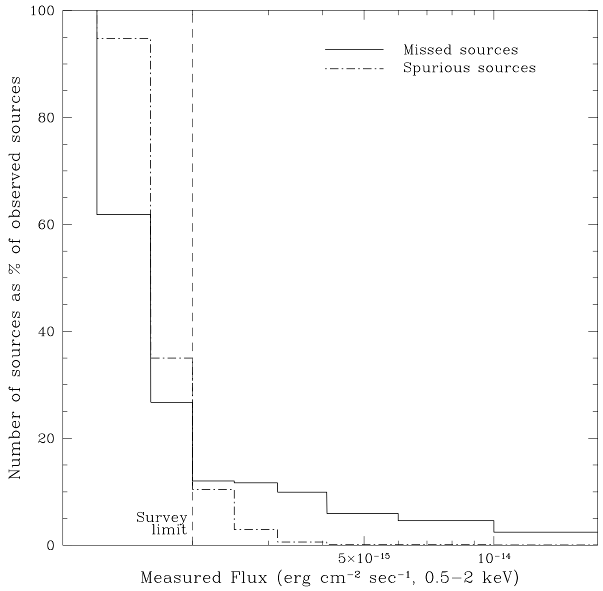

Figure 1. The percentage of sources expected to be missed in our survey as a result of source confusion and statistical noise, as a function of detected source flux. The flux bin size is varied so that a similar number of observed sources lie in each bin. The number of spurious sources expected is also displayed. These results are produced from simulations covering an area $\sim 250\times$ the area of the present deep survey. See text for further details of the simulations.

as a function of measured (ie observed) source flux. The bin sizes are varied in order to have approximately equal numbers of sources in each bin. Below 2×10^{-15} erg cm^{-2} s^{-1} the number of spurious sources rises rapidly. The number of missed sources also rises rapidly below that flux, which we therefore choose as our survey limit.

Above 2×10^{-15} erg cm^{-2} s^{-1} there are 96 sources in the full 15 arcmin diameter survey area (and there are 105 sources above a flux limit of 1.6×10^{-15} erg cm^{-2} s^{-1} although, of course, we are very incomplete at that flux limit). The distribution of these sources is shown in figure 2, in which figure we also show the shape of the 'complete area', which is described in section 4. There are 70 sources above a flux limit of 2×10^{-15} erg cm^{-2} s^{-1} in the complete area. The actual number of missed and spurious sources expected in the complete area is given in Table 1. Reassuringly, the total number of spurious sources down to a flux limit of 2×10^{-15} erg cm^{-2} s^{-1}, by which flux we expected to have detected $\sim$1 spurious source, is 2.

Above a flux of 2×10^{-15} erg cm^{-2} s^{-1} we miss a total of $\sim$ 7 real sources. We have examined many of the simulated source maps by eye and, in the large majority of cases, sources are missed because they happen to lie close to a brighter source, ie they are confused. The number of confused sources is approximately what one expects from 'back of the envelope' calculations. We can slightly decrease the number of missed sources by adjusting the parameters of the source searching algorithm, but only at the expense of detecting more spurious sources.

In addition to the loss of sources due to confusion, and statistical noise at low flux levels, we may lose a small number of the faintest sources at large off-axis angles where the psf is larger and the effective collecting area is less. The psf and effective area do not change by more than a few percent until one reaches 12 arcmin, the radius chosen by GBR to produce the source counts from the AO1 observation. However by 15 arcmin off-axis the effective area has dropped to 90% of its on-axis value for a typical 1 keV source. By taking into account how the psf increases, and how the collecting area of ROSAT decreases with radius, and the exact shape of our survey area, we have estimated how the effective area of our survey varies with flux and hence derived an approximate area correction factor. The correction is small, applies only at the very faintest fluxes and has little effect on derived source count slopes. Our best estimate is that the effective area of our spectroscopically complete survey area (figure 2) is about 30% lower than the geometric area at 2×10^{-15} erg cm^{-2} s^{-1} but that the effective area is the same as the geometric area by about 2.4×10^{-15} erg cm^{-2} s^{-1}. The fact that the area correction factor (ie not taking account of any confusion losses) cannot be much greater than 30% at the faintest fluxes is supported by the observation that the third faintest source in our list, source 133 which has a flux of 2.1×10^{-15} erg cm^{-2} s^{-1}, lies 11.6 arcmin off-axis and approximately 70% of our spectroscopically complete area lies within 11.6 arcmin of the axis.

2.2.2 Accuracy of Fluxes

In figure 3 we present the relationship between the fluxes of the 'real' and corresponding 'found' sources. The relationship is quite close to 1:1 but there are some minor deviations. In particular we notice that at high fluxes the measured fluxes are systematically slightly lower ($\sim$ 10%) than the input actual fluxes. The reason is probably associated with the marginally different psfs used in the creation of the simulated images and in the source finding algorithm. In order to create the simulated images we used an average 'observed' numerical psf. However, in order to greatly speed up the computational process, we used an analytic psf in the source searching procedure. Exactly the same analytic psf was used in the analysis of the real data and in the simulations. At lower fluxes the difference between the measured and actual fluxes becomes less and at the survey limit the mean measured flux just exceeds the actual flux

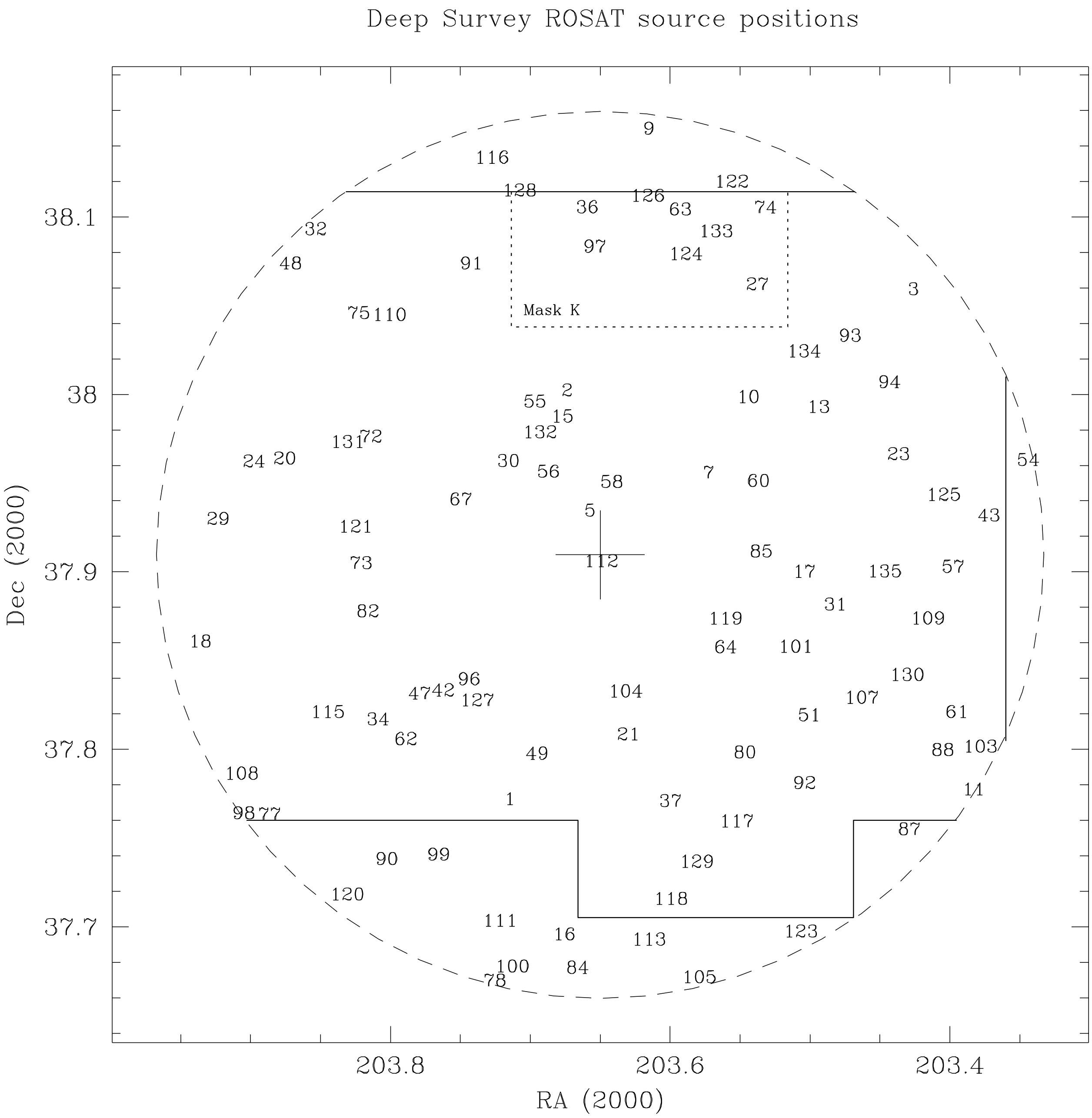

Figure 2. Map of the ROSAT source distribution with numbers identifying individual sources. Right ascension and declination are both given in degrees. Source 47 has been shifted west by 30 arcsec to avoid overlapping source 42. The solid lines delineate the area covered by our spectroscopically complete survey which includes 84% of the total 15 arcmin radius area (dashed line). To avoid a contrived area, only lines of constant right ascension or declination have been used in delineating the area. CFHT MOS Mask K is noted with dotted lines. If it is left out our complete area comprises 78% of the 15 arcmin radius area.

and the spread in measured flux for any input actual flux increases. At fluxes below the survey limit the measured flux substantially exceeds the actual flux. The rise in measured flux relative to actual flux at the lowest flux limits is well known (eg Hasinger *et al.* 1993) and provides an additional criterion for choice of the survey flux limit. As these systematic errors are small compared to the statistical errors in the fluxes, we do not correct any of our observed fluxes.

2.2.3 Positional Accuracy

In figure 4 we present the difference in position between the 'real' and 'found' sources, as a function of measured flux. We include all 'found' sources, independent of whether they are confused by the presence of a very close companion, and so the positional errors are a true representation of the positional errors in the actual survey sources. As the distri-

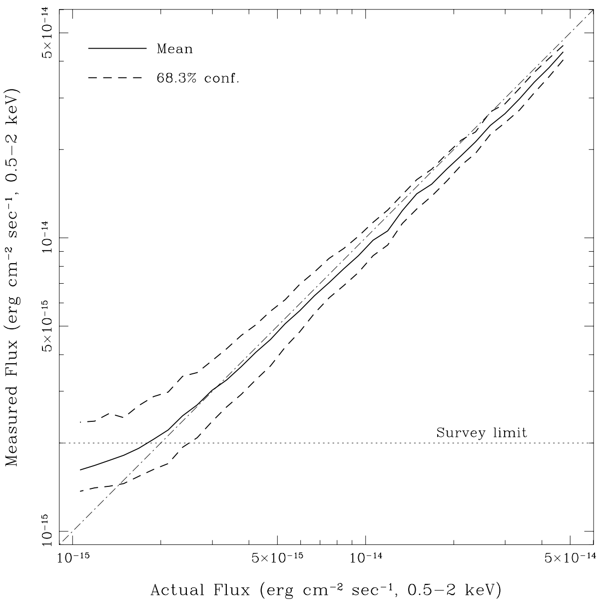

Figure 3. Fluxes of the 'real' (ie actual) and corresponding 'found' (ie measured) sources. The mean value and 68% confidence limits of the distribution are shown.

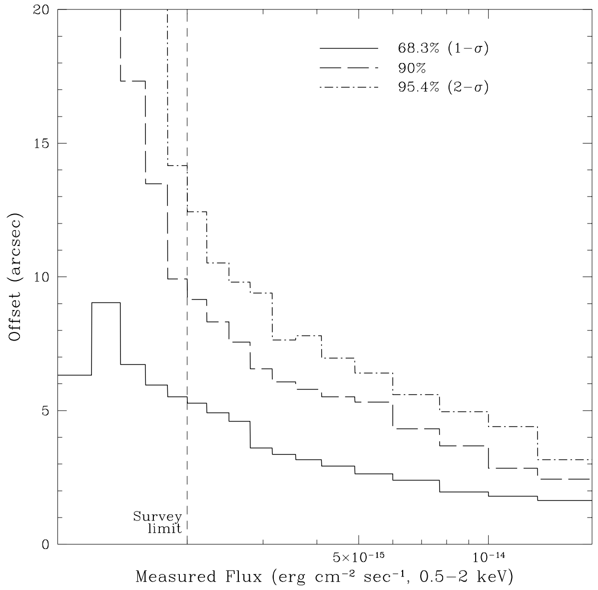

Figure 4. Offsets, derived from simulations, between 'real' (ie input) and 'found' (ie detected) source positions as a function of detected source flux. These offsets take proper account of the displacement of detected source positions caused by source confusion.

butions are not entirely gaussian, we present a number of different confidence regions for the offsets.

Our standard source searching algorithm does not vary the width of the psf, apart from as a function of off-axis angle, to take account of extended or confused sources. Examination of the simulated confused sources shows that, unless the two constituent sources are of similar flux, the source searching algorithm quite strongly favours the position of the brighter source. Thus the main effect of confusion is for sources to be missed rather than for the positions of detected sources to be grossly displaced.

When two sources of similar flux occur less than a beamwidth ($\sim$ 25 arcsec) apart, an extended source will be produced and, depending on the separation and flux of the individual components, the extension may be measurable and it may be possible to model the individual components. Although our standard source searching algorithm would only detect one source, we are able to perform a more sophisticated search for possible extension or multiple components in individual cases. We take account of source spectra as the psf of soft sources is larger than that of hard sources. We have not carried out a systematic search of all sources for extension but have examined sources for which there was some reason to consider extension. Examples include sources identified with clusters of galaxies or sources for which there was more than one good candidate identification. Initial source selection was performed by visual examination of the photon map. Visual examination is only effective when the photon counting statistics are good and so we only considered the brighter $\sim$half of our sources, down to source number 60. Of the 9 sources selected visually as being possibly extended (see notes on sources in section 4.1 for details), source 23 definitely consists of two separate sources of approximate flux ratio 2:1, source 34 is definitely extended and is almost certainly a distant cluster and 3 others (sources 5,9 and 51) have weak-to-reasonable evidence for a possible companion of flux considerably less than the primary source. The remaining sources (10,11,17,43) are all perfectly consistent with a single point source, although sources 10 and 11 are very soft and so the psf is large. In all cases of extended/multiple X-ray sources, the possible optical identifications are consistent with the X-ray results.

2.3 The Source Counts

In figure 5 we present the observed differential source counts. We compare the counts within 12 arcmin radius (solid line), where the area correction factor has no effect, with those within the selected area (dotted line) and those out to the full 15 arcmin radius (dashed line). No corrections have been applied for confusion or reduced effective area at low fluxes. If the area correction factor were applied, it would only affect the lowest flux bin, raising its value in the 15 arcmin radius and selected area cases to almost exactly the same as that of the 12 arcmin counts. To avoid cluttering the diagram errorbars have not been applied but, for the differential plot, they are simply 'root N' errors based on the numbers of objects in each differential bin and easily cover the minor differences between the three source counts. Thus we confirm that the area correction factor has little effect on the overall source counts.

In figure 6 we present the uncorrected integral source counts from the full 15 arcmin radius area. For comparison with previously published counts we follow GBR and also show the best fit to the source counts of Hasinger *et al.* (1993). Given that our sources are presented as raw data

Table 2. DIFFERENTIAL SOURCE COUNT SLOPES AT FAINT FLUXES: $2-16\times10^{-15}$ **ergs cm^{-2} s^{-1}**

	Selected Area	Full 15' radius	GBR	Hasinger93*
Uncorrected	$-1.42^{+0.19}_{-0.26}$	$-1.65^{+0.16}_{-0.28}$		
Corrected for Missing Area	$-1.46^{+0.19}_{-0.28}$	$-1.73^{+0.17}_{-0.29}$		
Corrected for Missing Area and Confusion	$-1.53^{+0.19}_{-0.28}$	$-1.80^{+0.17}_{-0.25}$	-1.78 ± 0.38	-1.94 ± 0.19

* Note that Hasinger *et al.* (1993) determine a higher break flux (2.66×10^{-14} ergs sm^{-2} s^{-1}) than the present work and so are expected to measure a steeper source count slope.

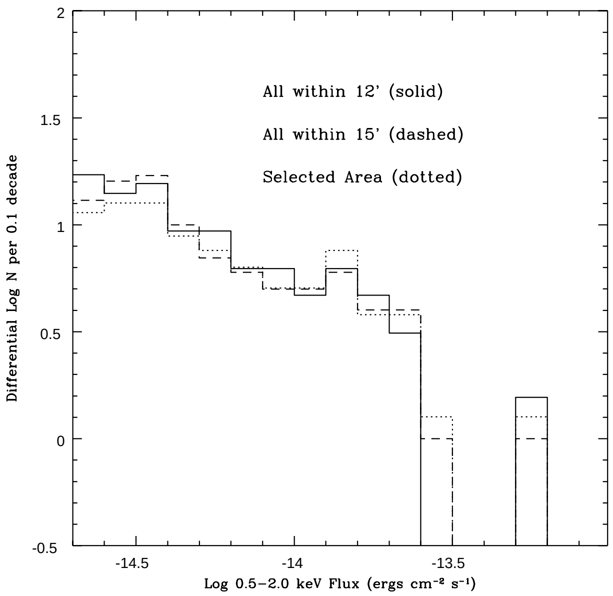

Figure 5. Differential source counts for sources within the full 15 arcmin radius X-ray survey area (dashed line), for sources within 12 arcmin (solid line) and for sources within the spectroscopically complete area (dotted line). All source counts have been normalised to the full geometric area of the 15 arcmin radius X-ray survey area. No corrections have been applied for confusion or for slight incompleteness in the 15 arcmin and complete area counts in the lowest flux bin.

whereas, following GBR, Hasinger *et al.*'s counts are presented as a smooth best fit, we see very good agreement between the datasets. Our source counts drop below those of Hasinger *et al.* at the highest fluxes shown because, unlike them, we have not corrected for the fractional lack of very bright sources of very low surface density which are not found in the small area of our survey. We can see that both the integral and, more importantly, the differential source counts, continue down to 2×10^{-15} erg cm^{-2} s^{-1} as a smooth extrapolation of the source counts derived by Hasinger *et al.* , and GBR, at slighly higher fluxes $\sim 3\times10^{-15}$ erg cm^{-2} s^{-1}, in agreement with the source counts derived from fluctuation analysis by Barcons *et al.* (1994).

Both GBR and Hasinger *et al.* fit the integral source counts with separate power laws at faint and bright fluxes. GBR measure the break flux between the two power laws to be 1.6×10^{-14} erg cm^{-2} s^{-1} and the slightly deeper data presented here confirm that break flux. Because of our incompleteness at bright fluxes we do not attempt to measure the source count slope above the break flux. However below the break flux we determine the source count slope by maximum likelihood fitting to the differential source counts in the flux range 2 to 16×10^{-15} erg cm^{-2} s^{-1}. The results are presented in Table 2. We can see that none of the correction factors have much effect and that our fully corrected results are in excellent agreement with the earlier measurement of GBR. They are also in good agreement with the result of Hasinger *et al.* given that Hasinger *et al.* determine a higher break flux (2.66×10^{-14} erg cm^{-2} s^{-1}) and, as we move the break flux to higher fluxes, we move onto the steeper part of the integral source counts. We note that the differential slope for the complete area is flatter than that for the full 15 arcmin counts at about the 1σ level. The difference just reflects the random distribution of sources within the 15 arcmin radius area. If we rotate the complete area by 90°with respect to the sky we will include the faint sources which we presently miss to the south and the source counts will be steeper than those of the full 15 arcmin area.

3 OPTICAL OBSERVATIONS

3.1 CCD Photometry

The initial optical identification of the X-ray sources was made using V and R band CCD observations of the survey area from the 88 inch University of Hawaii Telescope and the 2.4m Michigan-Dartmouth-MIT (MDM) Telescope in May 1992 and June 1993. The observations were typically of 10 minutes duration and reached R=23 mag. Seeing was typically 1 arcsecond. Subsequently the whole field was observed in the I band with the 2.4m MDM Telescope and using the Hitchiker Camera on the 4.2m William Herschel Telescope (WHT) on La Palma; the resultant observations were of similar depth and resolution to the V and R band observations and will be discussed elsewhere. Somewhat deeper observations (R=24) were made on the WHT at the auxiliary focus of some fields which were blank on the initial CCD images. Optical coordinates were determined to better than 0.5 arcsec by cross-referencing the CCD coordinate frame to that of FK4 stars determined from scans of the Palomar Sky Survey plates by the Cambridge automated plate measuring machine (APM).

In March 1995, we observed the whole ROSAT survey region again in the R band on the Canada-France-Hawaii telescope using the University of Hawaii 8K x 8K CCD array (Metzger *et al.* 1995). This device enabled us to observe the whole 15 arcmin radius area at the same time, with 0.22 arcsec pixels. A total of approximately one hour of integration time was obtained in sub-arcsecond seeing conditions resulting in a limiting magnitude of R $>$ 24.

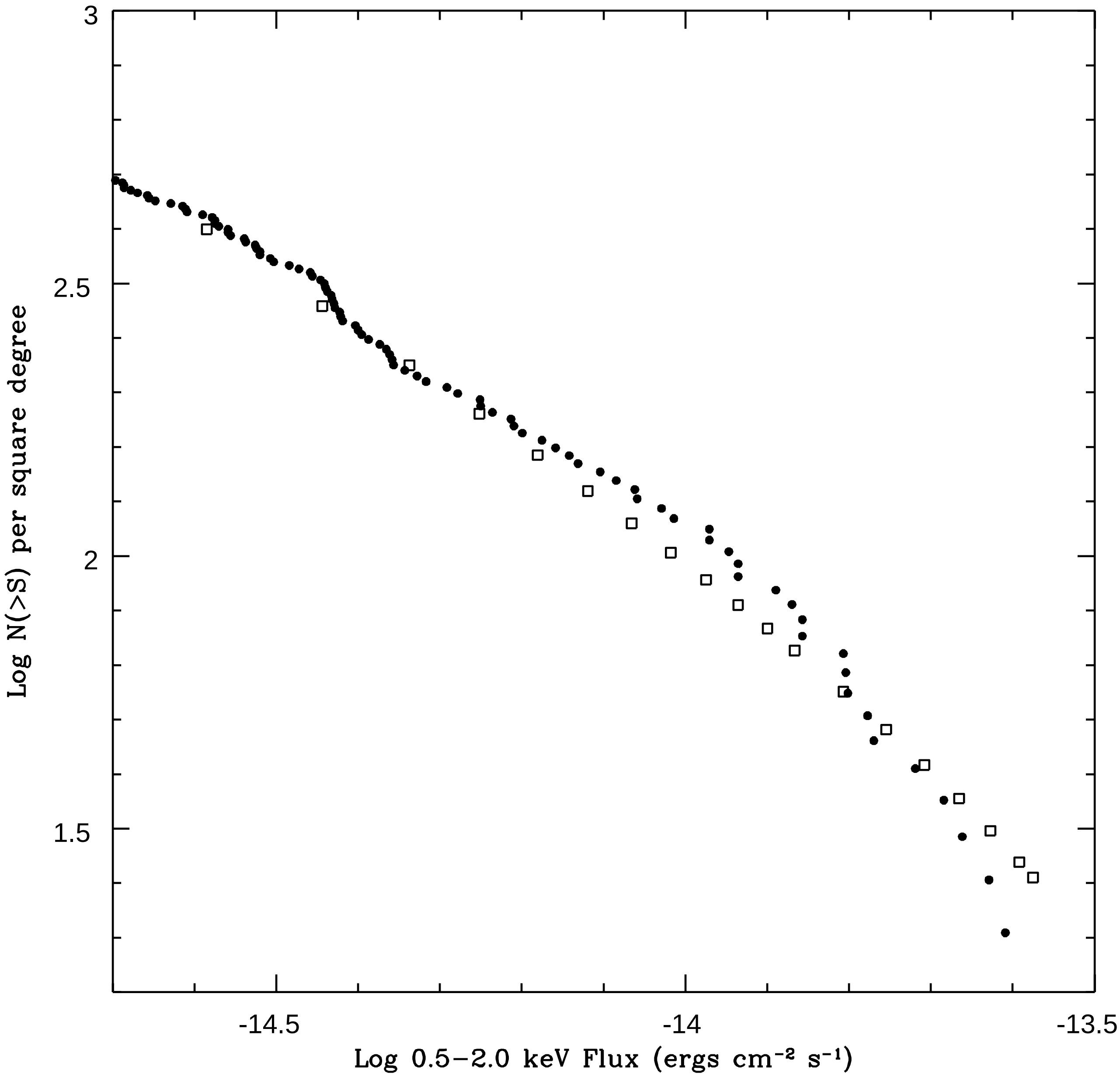

Figure 6. Integral source counts from the full 15 arcmin radius area (filled circles) compared with the best fit to the source counts derived by Hasinger *et al.* 1993 (open squares) from a similar ROSAT PSPC survey. Note that Hasinger *et al.* correct for incompletness at the high flux end caused by the small area of their (and our) survey whereas we do not. Also we plot our raw data but a (smoother) best fit to Hasinger *et al.* 's data.

3.1.1 Registration of X-ray and Optical Coordinate Frames

A correction for the ROSAT roll angle error of 0.185 degrees (Briel *et al.* 1995) was applied initially. Subsequently, in order to align accurately the X-ray and optical images, three independent methods were used to measure the small ROSAT PSPC systematic position error. X-ray positions were compared to (a) positions determined from APM measurements of Palomar plates of the first few definite spectroscopic identifications which we obtained in our initial spectral observations at the NOT and UH 88" telescopes in 1992 (see section 3.2), (b) APM positions of the few bright optical stars coincident with X-ray sources, (c) VLA positions of the 11 X-ray/radio coincidences. All three methods gave a consistent offset of 13 ± 1 arcsec which was removed from all X-ray positions, leaving only the statistical uncertainty which has been discussed above (figure 4). Most ($\sim 90\%$) of the X-ray sources were then identified with objects brighter than R=23 mag. R magnitudes were determined for all optical objects within 30 arcseconds of the X-ray positions and the magnitudes of likely identifications are listed in Table 3.

3.2 Spectroscopy

Low resolution $(10-15\text{Å})$ spectra of 10 of the brightest optical candidates were obtained on the NOT and on the UH 88" telescope in May 1992 and June 1992 respectively. The UH spectra covered 4000-9000 Å and the NOT spectra covered only 6000-9000 Å but were adequate to confirm and classify the identifications and hence enable us to tie our X-ray coordinate frame to the optical frame. Subsequently spectra of the majority of the remaining fainter optical candidates were obtained with the Multiple Object Spectrograph (MOS) on CFHT and the ISIS spectrograph on the WHT. With MOS we used grism O300 in first order with Loral 3 as the detector, covering $4000-9000$Å with ~ 15Å resolution. Approximately 15 spectra were taken at a time. Data were analysed using IRAF. Observations with ISIS were made in single long-slit mode to cover objects in gaps between MOS masks. ISIS covered a similar wavelength range to MOS with slightly better resolution. In the red and blue arms of ISIS we used gratings R158R and R300B respectively, with the 5400 dichroic, and Tektronics CCD detectors in both cases. With both MOS and ISIS multiple exposures were made to enable cosmic ray events to be identified and removed. The typically slit width was 1.5 arcsec. Flux standards were observed and we observed at the parallactic angle whenever possible (the large majority of cases) to avoid gross distortions of the spectral shape.

4 THE OPTICAL IDENTIFICATIONS

As a result of the above observations we are able to define a sub-area comprising 85% of our full 15 arcmin radius survey area in which we are nearly spectroscopically complete. The outline of this area is shown in figure 2, together with the distribution of sources. The shape of the sub-area is based on the distribution of CFHT MOS masks. We have drawn the shape in as unbiased a manner as we can, using only NS or EW lines to avoid producing a contrived shape. Thus we include a small number of sources for which we have not yet obtained optical spectra. We note particularly a mask which we label as 'mask K'. Conditions were somewhat worse than normal during the observation of mask K and so we have only obtained identifications for 4 of the 8 sources covered by mask K. For the present purposes we do not include the mask K sources in our statistical analysis, thereby reducing our complete survey area to 79% of the complete 15 arcmin radius, ie 0.155 square degrees. However all mask K sources are noted in Table 3 so that readers may reproduce the source counts with those sources included, if they wish.

The process of optical identification is based primarily on the positional coincidence between the X-ray source and the optical candidates. For sources in the brighter half of our list we generally require an X-ray/optical offset of less than 10 arcsec but for sources in the fainter half of the list we relax the positional criterion slightly to ~ 15 arcsec. The second criterion is optical magnitude - objects brighter than R=21 are sufficiently rare that they are likely candidates but objects of R$\geq$ 23 are not unusual. For the brighter sources there was usually only one reasonable candidate satisfying the above criterian but for the fainter sources there was sometimes more than one. A tertiary criterion was morphology. We had initially expected that almost all of the X-ray sources would be identified with QSOs and so even if there was a galaxy of $R \leq$21 located close to the X-ray centroid, we also took optical spectra of possible stellar candidates at fainter magnitudes and at X-ray/optical offsets greater than we considered reasonable (> 15 arcsec) for an identification. Almost all of these stellar candidates turned out to be stars and most were ruled as unlikely identifications on the basis of their X-ray/optical ratios (eg Stocke *et al.* 1991).

We took spectra of the likely candidates objects to R=22 mag and the results are discussed in detail in Section 4.1, and are tabulated in Table 3. When an identification is considered certain it is flagged with a '*' in column [o] of Table 3. Likely, but less certain, identifications are flagged as '(*)' and possible identifications have no flag.

We have defined a number of source classes. Stars are labelled with their approximate spectral type. QSOs are defined as having broad (FWFM >1000 km s^{-1}) emission lines and $L_X > 10^{43}$ ergs s^{-1} ($H_0 = 50$ km s^{-1} Mpc^{-1}, $q_0 = 0.5$). Galaxies are divided into absorption line systems ('galaxies') and those with narrow (FWFM <1000 km s^{-1}) emission lines (NELGs). There are also a small number of groups or clusters of galaxies. "?" means there are no useful spectra of objects in the errorbox and "blank" means that there are no objects brighter than R=23mag in the errorbox.

Of the 96 sources of flux $\geq 2.0 \times 10^{-15}$ erg cm^{-2} s^{-1}, 70 lie within our sub-area (or 78 if we include mask K). However in order to make the data as useful as possible to other researchers the photometric data for all sources, and spectroscopic results for all sources for which data are available, including some outside the complete area but within the original 15 arcmin radius survey area, are listed in Table 3. It is hoped that other observers may be able to add to the identifications and, should they do so, we would be grateful if they could contact us so that we may update Table 3 and eventually publish a completely identified version. Where there is anything of interest in the optical or X-ray field over and above the simple identification information given in Table 3, notes are given below. The notes concentrate on sources within the complete sample.

The sources are arranged in count rate order (which very closely matches the flux order) so that the distribution of identification class with flux can be seen clearly. It will be noted that not all source numbers are present. This is because our original source list comprised all sources out to 20 arcmin radius but we have ignored those beyond 15 arcminutes in our subsequent analysis. As the source number is merely a label we choose to keep the original source number to avoid any possibility of mixing sources up.

4.1 Notes On Individual Sources

2 Broad line radio galaxy. Extended radio emission. Has an extremely high hardness ratio. The source certainly is very hard, perhaps indicating some absorption above galac-

Table 3. SUMMARY OF X-RAY AND OPTICAL OBSERVATIONS

[a]	Our source number.
[b]	Observed 0.5-2.0 keV counts per 10,000s.
[c]	0.5-2.0 keV flux corrected for off-axis angle.
[d]	Hardness ratio, ie the ratio of counts in the 0.5-2.0 keV band to those in the 0.1-0.5 keV band. See section 5 for details.
[e,f]	RA and Dec (J2000) of the X-ray centroid.
[g]	Off-axis angle of the source (arcmin).
[h]	"R" indicates that the source is detected in the preliminary 20cm radio map.
[i,j]	RA and Dec of optical object. In most cases this object is the most likely optical counterpart but where the optical counterpart is uncertain the object listed may be simply the brightest optical object in the errorbox, or the object nearest the X-ray centroid. In the least certain cases no optical coordinates are given. Where there is the possibility of X-ray emission from more than one optical object, the probable dominant emitter is listed. See notes for more details.
[k]	"-" means not in complete sample. "K" means from CFHT mask K.
[a]	Repeat of source number.
[l]	X-ray/optical offset (arcsec).
[m]	R-band magnitude.
[n]	Identification class.
[o]	Confidence of the identification. "*" means certain, "(*)" means likely, blank means possible.
[p]	Redshift.
[q]	"Y" means notes are given below.

tic, but the hardness ratio may be overestimated due to the difficulty of detecting the source in the soft (0.1-0.5 keV) image as it is very close to the very soft source, 15.

5 The X-ray source, appears pointlike, with a very weak extension to the south-west. Fitting the image weakly supports the visual impression. The optical field within an arcminute of the X-ray centroid contains 6 fairly bright spiral and elliptical galaxies (R $\sim$ 18) and a large number of fainter galaxies (R<20) which may be a distant rich cluster. The brightest objects within the 10 arcsec radius errorbox are two elliptical galaxies of R=20.1 and 21.5 respectively, the brighter of which looks like the brightest galaxy of the distant cluster. The fainter galaxy has a probable redshift of 0.57 with possible very weak [OII] emission. There are no strong features in the spectrum of the brighter galaxy and we are not able to determine its redshift. NOTE that the redshift given in Table 3 is the redshift of the fainter galaxy, not the galaxy whose position is listed in Table 3, on the assumption that both galaxies are members of the apparent distant cluster. Two of the brighter (foreground?) galaxies have measured redshifts, both being 0.247, and one spiral shows H_α and [SII] emission. None lie within the errorbox. The most likely identification is therefore with the distant cluster with the more nearby non-X-ray emitting group superposed. The weak extension overlays another group of 21mag galaxies which may be part of the distant cluster, but no redshifts are available. Note however that the overall hardness ratio of the whole source (H=0.37) is too low for all of the emission to be explained by hot cluster gas and requires some contribution from a steep power-law (ie AGN) - see Table 6.

9 This source is nearly at the edge of the 15 arcmin field, and is also very soft, more consistent with AGN-like emission. Even so, there is some evidence for extension with a weak component to the west. There are no candidates within 10" of X-ray centroid but there are some 21mag compact objects at 10-20" with the nearest listed in Table 3. The weak X-ray component overlays a relatively bright (17 mag) stellar object $\sim 30''$ west of the X-ray centroid. No useful spectra have been obtained.

17 Visual inspection of the X-ray image appears to show a faint extension to the south, overlaying a 20 mag elliptical galaxy. However the X-ray flux of the extension is below the survey limit, and fitting of the image provides no statistical evidence of extension.

23 The X-ray image is definitely extended and provides our strongest statistical case of confusion. The image is best fit by two point sources separated by 20-30" along a NE-SW axis. Approximately 2/3 of the counts come from the southern source which overlays the 20.4 mag QSO listed in Table 3. The fainter source overlays a 17.7 mag elliptical galaxy with weak [OIII] and H_α emission. The coordinates of the galaxy are RA 13 33 45.35, Dec 37 58 07.7 and its redshift is 0.175. Although we have not included it in our complete sample of NELGs, this galaxy does have a valid claim to be included. The overall source spectrum is rather soft, consistent with the majority of the counts coming from the QSO.

29 Although slightly further from the X-ray centroid than expected (13.7"), there are no other likely identifications. The X-ray position is pulled to the NW by a nearby source (154) which, although real and identified with a redshift 2.278 QSO, is below the flux cut-off for this catalogue.

30 Note that the redshift of this QSO is identical to that of the QSO identified with source 56 which is 2 arcmin away.

32 The X-ray centroid is coincident with the brighter of 2 interacting spiral galaxies. Both have the same redshift and both show narrow emission lines.

34 The X-ray source is best fit by an extended source. A reasonably compact group of faint (21 mag) galaxies lies within the errorbox, confirming the identification with a distant cluster of galaxies. We have spectra of two galaxies. Neither show strong emission lines. The spectra are not of sufficient quality to determine a definite absorption line redshift but we make a tentative estimate of 0.595 based on possible H+K and G-band. The relatively hard spectrum (H=0.86) is in agreement with the identification with a cluster.

42 Interacting galaxy. Measured position of X-ray source is probably displaced from its true position towards neighbouring source 47 (and away from the optical galaxy). Note source 47 is at the same redshift. There are many galaxies in this field.

43 Narrow line radio galaxy. Member of a rich cluster whose centre is approximately 80 arcsec south of this galaxy. We have spectra of 4 more galaxies all with redshift 0.383. A source which shows up only in the soft band (0.1-0.5 keV), and so is not listed here, is coincident with the cluster centre.

47 Measured position of X-ray source is probably displaced from its true position towards neighbouring source 42 (and away from the optical galaxy). Note source 42 is at the same redshift. There are many galaxies in this field.

49 We give the coordinates of the brightest galaxy within the 10" radius errorbox. We can only detect absorption features. At such a high redshift (0.709) the luminosity ($> 10^{43}$ ergs/s) implies emission from a group or poor cluster rather than from an individual galaxy. However, perhaps not unexpectedly, a rich cluster is not visible on our CCD images. We also note a bright (R∼18) K star at Δ_{X-O}∼20" to the southwest. For a relatively bright source only 7 arcmin off axis, 20" is much further from the errorbox centre than we would expect for a real identification, however the star is quite bright so cannot be entirely ruled out. The source is not detected in the soft band (0.1-0.5 keV), which is quite consistent with the hard spectrum expected from a cluster.

51 The X-ray source is slightly extended ($\sim 30''$) in a NW-SE direction, consistent either with an elliptical source or with the existence of a fainter companion source to the SE of the X-ray centroid. Optically the field is crowded. The most likely identification is with a bright (16.4mag) narrow line elliptical radio galaxy, redshift 0.061, which lies ∼ 16 arcsec east of the X-ray centroid. However a group of six 18-19 mag galaxies lie 10-40" from the centroid along the extension of the X-ray source. Two of these have the same redshift (0.257 - absorption line) so weak emission from the group may be responsible for the X-ray extension. There is also another narrow emission line galaxy at redshift 0.025 (not a misprint), 40 arcsec NW of the X-ray centroid, lying just at the edge of the X-ray extension.

54 No candidates brighter than 23 mag within 10 arcsec; nearest object is stellar, R=19, at 20 arcsec. No spectra have been obtained. Note large off-axis angle.

56 Note that the redshift of this QSO is identical to that of the QSO identified with source 30 which is 2 arcmin away.

58 A second redshift is available in this cluster, 0.307. The X-ray source is complex/extended. It is not detected in the soft (0.1-0.5 keV) band, which is consistent with the hard spectrum expected from a cluster.

60 An object of R=22.7 which is either a galaxy of high central surface brightness or possibly a QSO is dead centred (Δ_{X-O}= 1.4 arcsec) in the errorbox and is a reasonable candidate identification as the next nearest object is a galaxy on the edge of the errorbox (Δ_{X-O}=11 arcsec) of R=21.6. The R=22.7 galaxy shows narrow emission lines at 5900 and 6565Å which may be badly subtracted night sky NaD and H_α, but we note that the 5900 line is over twice as strong as the 6565 line and that the very strong [OI] 5577 night sky line subtracts out perfectly. No broad emission features are detected. Alternatively, the 5900 line may be real. If it is [OII] 3727, this may be a high redshift (z=0.58) NELG. The brighter galaxy on the edge of the box displays only one narrow line at 6600Å. This line is seen independently in spectra from CFHT and from the WHT. If it is [OII] 3727, the redshift is 0.76. The source is harder (H=0.86 ± 0.23) than expected from a QSO-like power-law spectrum but, on the other hand, does have a high X-ray/optical ratio (see figure 17), more consistent with a QSO than a starburst galaxy.

62 Large R=18.6 elliptical galaxy 9 arcsec from X-ray centroid. No emission lines. Redshift 0.251. There are a lot of nearby fainter (22mag) galaxies and a few other brighter (R∼ 19) galaxies. The R=18.6 galaxy may be the dominant galaxy in a group.

73 A 23mag galaxy is well centred (Δ_{X-O}=4.7). The nearest object noticeably brighter is a 20mag stellar object (Δ_{X-O}=20").

74 Identical absorption line redshifts of 0.382 exist for both a galaxy well within the errorbox and one just outside it.

77 Group of galaxies. A second galaxy with a similar absorption line spectrum has a close redshift (0.304).

78 The nearest object to the X-ray source is listed in Table 3 (R=22.07, Δ_{X-O}=15 arcsec). A galaxy of R∼ 21 lies further away ($\Delta_{X-O}\sim 25''$). However note large off-axis angle. The field is just off the edge of our deepest CFHT images. No spectra were obtained.

80 The errorbox is empty apart from a 23mag compact object at Δ_{X-O}= 2.7" and the surrounding field is also very empty so this object is the most likely identification. The low signal/noise spectra are reasonably clear of poor night sky subtraction features but there is one emission line at ∼ 4940Å which is visible on spectra taken in 1994 and 1995. If this is [OII]3727 the redshift would be 0.327.

82 A reasonably compact object of R∼ 23.5 is visible on the deepest CFHT and WHT auxiliary port images very near the centre of the errorbox.

84 The nearest object to the X-ray centroid is a 20.1 mag compact object at Δ_{X-O}=13.7". No spectra are available and the source is just off the edge of our deepest CFHT image. Note large off-axis angle.

85 The 20.7 mag galaxy listed is the brightest object in the errorbox. It is at Δ_{X-O}=5.1". The only other object brighter than R=23 in the errorbox is an R=22.2 mag object, to the north of the 20.7 mag galaxy, at Δ_{X-O}=7.8". We cannot tell if the fainter object is a galaxy or a star and no spectra are available.

87 The coordinates and magnitudes given are of the nearest bright (R<23) galaxy. Note large off axis angle.

88 The identification is unclear. There are two 21mag objects within 3" of the X-ray centroid. One is stellar, the other is slightly fuzzy. The spectra are of poor S/N with no really strong features. A 21mag Mstar lies at Δ_{X-O}=9", but is too faint optically to be a likely identification. In Table 3 we give the coordinates of a 17mag K star at Δ_{X-O}=14" which is just about bright enough optically to be a reasonable identification but is rather further from the errorbox centre than we would expect for a real identification.

90 There is only one possible candidate, a 21mag slightly fuzzy stellar object at Δ_{X-O}=2.2". There is no spectrum but it is probably a QSO.

93 The galaxy listed is the only object brighter than R=23 in the errorbox.

94 H_α is slightly broadened (FWHM=1000 km/s). This is a narrow line radio galaxy.

96 The X-ray source is coincident with the centre of a reasonably rich cluster. The redshift given is that of the brightest galaxy, a large elliptical, 11 arcsec from the X-ray centroid. The elliptical shows no optical emission lines but does host an extended radio source. Some contribution to the X-ray emission from an active nucleus cannot therefore be ruled out.

97 The brightest object within 20 arcsec of the X-ray centroid is a 22.7mag compact galaxy, with faint extension to NW, 6 arcsec from the X-ray centroid. This may be a low redshift QSO, however no optical spectrum is available.

98 An elliptical galaxy with a bright nucleus, which appears to be the brightest in a cluster is near the centre of the errorbox (Δ_{X-O}=3.7"). Based on possible H and K the redshift is 0.255. There is a hint of [OIII] emission but it is right on top of the 6300 night sky line and so may not be real. No other features are visible.

99 The brightest galaxy in the errorbox is $\sim$ 23 mag with a suspicion of a bright nucleus. A possible extremely distant, but quite rich, cluster with all galaxies of R=23 or fainter is centred about 20 arcsec south of the X-ray centroid.

100 There is nothing brighter than 23 mag within 10" of the X-ray centroid but there are two somewhat flattened 20mag galaxies on opposite sides of the box, each of Δ_{X-O}=20". Note the large off axis angle. There are no spectra.

105 A compact group of 3 bright galaxies lies within the errorbox, two very close together; a fourth lies just outside. The coordinates of the brightest are given. No spectra were obtained.

107 There is nothing brighter than R=23.5 within 10". There are a number of 21 mag galaxies slightly further away and the coordinates of the nearest is given. We have low S/N spectra of three of them but cannot distinguish any features. There is also a much brighter galaxy ($R \sim 16$) about 30" north of the errorbox, but, although very bright, it is too far away to be a reasonable candidate for a source only 10 arcmin off axis.

109 This is a complicated region. There are two other sources (which we know as 170 and 169) which are detected only in the 0.1-0.5 keV band, lying 30 and 70 arcsec northeast respectively of source 109. Likely identifications of sources 169 and 170 are an M star and a z=0.256 NELG. Also to the NE, at Δ_{X-O}=$\sim$20" is a z=2.12 QSO, which may be the identification of source 109. The nearest object brighter than R=23 to source 109 is a 21.9mag absorption line galaxy of probable redshift 0.226 at Δ_{X-O}=12", to the NE but this is unlikely to be the identification.

112 There is nothing brighter than R=23 within 10". The coordinates given are of the nearest object, an R=21.7 galaxy but this is too far (16") from the X-ray centroid for a source almost on-axis to be a reasonable identification. The spectrum is of poor S/N.

113 There is a group of 3 faint (R$\sim$ 23) galaxies within 10". The coordinates of the brightest is given. There are 2 brighter (R$\sim$ 21.3) galaxies both at Δ_{X-O}=15", one to the north, one to the southeast. There are no spectra.

116 The coordinates given are of the brightest galaxy within 10". It appears to be a double/interacting galaxy. There is nothing brighter than 21mag within 40". No spectra were obtained.

119 Within 10" there is a 17 mag K star at Δ_{X-O}=8" and a 20 mag absorption line galaxy at Δ_{X-O}=4" with a possible redshift of 0.368. Both are possible candidates. There is no indication of a group or cluster of galaxies.

120 There are quite a few very faint (R$\sim$ 23) galaxies nearby. The coordinates of the nearest bright (R>21) galaxy are given. This is a possible cluster candidate. No spectra were obtained.

122 There is one 21mag galaxy at Δ_{X-O}=18" south and another at Δ_{X-O}=$\sim 22''$ to the northeast. Given the large off axis angle and faint flux, these are feasible candidates. There are no spectra.

123 There are a couple of very faint (R$\sim$ 23) galaxies within 10" but more likely candidates are two 20.5mag stellar objects both at Δ_{X-O}=20", one to the north and the other to the south (listed in Table 3). There are no spectra.

124 There is a 21.7mag galaxy at Δ_{X-O}=5" (poor spectrum) which is a possible identification, as is a 16.4mag stellar object at Δ_{X-O}=18" (no spectrum) to the south and a 19.9mag M star at Δ_{X-O}=19" to the southwest.

126 A number of faint (R>22) galaxies around the errorbox. The only object brighter than 22mag is what looks like an R=$\sim$ 21 disc galaxy with smaller companion at $\Delta_{X-O}\sim$ 20", to the south. There are no spectra.

127 A 20mag galaxy with quite bright nucleus showing strong H_α and [SII] but H_β is not detectable and [OIII]5007 is very weak, lies at Δ_{X-O}=9" to the southeast (coordinates given). It is a weak VLA radio source. This is a likely identification but some contribution from a 19.7mag M star, 13" to the northwest cannot be ruled out. Note the very similar redshift of this galaxy to the nearby cluster identified with source 62. Two further galaxies with identical redshifts, one of which is also a weak radio source but neither of which is an X-ray source, also lie in the same general area.

128 A likely identification is with a 19mag absorption line disc galaxy with a bright nucleus at Δ_{X-O}=6". The only other possible candidate is a 20.7mag object which is either a very compact galaxy or a QSO/star at Δ_{X-O}=15" (poor spectrum).

129 Although the galaxy is not particularly bright, the spectrum is of good quality and many emission lines are visible including [OII], [OIII], H_α, [SII] but not H_β.

130 A very empty field. The nearest object brighter than R=23.5 to the X-ray centroid is probably a galaxy of R$\sim$ 22 at Δ_{X-O}=20" to the southwest.

131 Strong narrow [OII] and [OIII] emission lines are detected from the listed galaxy, which is diffuse, with a nearby fainter companion. It is a reasonable candidate but a more compact object, probably also a galaxy, of similar total magnitude and at a similar distance east of the X-ray centroid cannot be ruled out. (We do not have a good spectrum of the latter object.)

132 X-ray source is centred (Δ_{X-O}=5") on the brighter of two interacting galaxies. Both galaxies have the same redshift. The brighter galaxy shows moderately strong H_α and [SII] emission but weak or absent [OIII]. The spectrum of the fainter galaxy (R$\sim$ 21) is similar, but of poorer quality; H_α is right at the end of the spectrum and is weaker, if present at all.

133 The most likely identification is with a 20.6mag stellar object 9" south of the X-ray centroid. There is nothing else brighter than 22mag within 20". In terms of optical/X-ray fluxes, a QSO is more likely but an M star is possible. No spectra were obtained.

134 As almost the faintest source in the list, the offset of the NELG from the X-ray centroid (22 arcsec) is just about consistent with the NELG being the identification. The offset is larger than expected for a typical source at this flux but there is nothing brighter than 23.5 mag any closer to the X-ray centroid.

135 The listed 20.6mag galaxy at Δ_{X-O}=13" has a strong narrow emission line spectrum ([OII], H_β, [OIII]4959

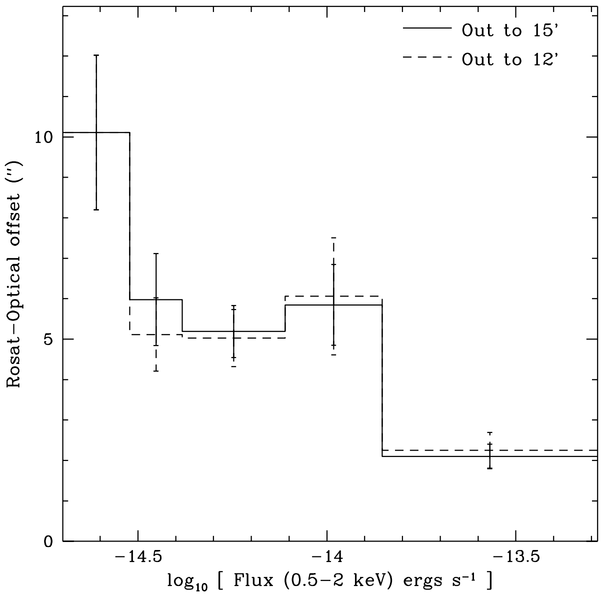

Figure 7. Average offset between the X-ray centroid and the optical identification, as a function of X-ray flux. The solid line represents the complete sample out to 15 arcmin radius and the dashed line is the restricted sample out to 12 arcmin. In the lowest flux bin the dashed and solid lines lie at exactly the same offset as all the sources in that bin lie within the 12 arcmin radius.

- 5007 is in night sky A band, H_α) and is the most likely identification. Another fainter galaxy lies very close to it. However a 20.3mag Mstar, also at Δ_{X-O}=13" cannot be ruled out. The surrounding field is somewhat richer than average in galaxies.

4.2 X-ray/Optical offsets for QSOs and NELGs

The accuracy of our X-ray positions is defined fundamentally by the simulations shown in figure 4. However a consistency check is provided by the average X-ray/optical offsets of identifications as, besides position, secondary criteria such as spectral type and morphology are taken into account before optical candidates are classed as reasonable identifications. We present these offsets, as a function of flux, in figure 7 for the firmest (ie '*') identifications. For this purpose we ignore clusters and groups as their X-ray centroid is not always well defined, and we ignore the '(*)' identifications as, in some cases the reason that the identification class is '(*)' rather than '*' is because of a suggestion of a weak companion source which might, of course, affect the position of the X-ray centroid. However including the '(*)' sources has little effect on the distribution. Reassuringly, figure 7 agrees quite closely with our simulations (figure 4).

We have separately computed the offsets for sources out to 12 arcmin and those out to 15 arcmin. We see little difference in the distributions, implying that flux, rather than offset from the field centre, is the main factor affecting positional uncertainty. Note, however, that in the very faintest flux bin we have no sources and hence no identifications beyond 12 arcmin.

Interestingly we note that, if we consider only the middle of our flux range which is equally populated by QSOs and NELGs, the mean distance of the optical identification from the errorbox centre is 4.8 ± 0.7 arcsec for the QSOs and 7.4 ± 0.8 arcsec for the NELGs. Although both offsets are well within the offsets expected for real identifications, the difference is significant at greater than 95% confidence using the Student t-test. One possible explanation of the difference is that the small number of expected incorrect identifications of NELGs has increased the average NELG offset whereas there will be almost no incorrect identifications with QSOs (for QSO number counts see, eg, Hall *et al.* 1996). Alternatively we note that previous ROSAT PSPC observations of bright nearby Seyfert 2 galaxies (Turner *et al.* 1993) have shown a factor of 8 enhancement of faint X-ray sources (typically 5-50% of the Seyfert 2 flux) within 100 kpc. The nature of these companion sources is not yet known but, if similar sources surround our NELGs, their fluxes would be below our detection limit but their effect would be to shift the centroid of the NELG X-ray emission by a few arcsec. We note that many of the NELGs in the present survey are in interacting systems (see notes on individual sources above). In a small number of cases we see emission line spectra from the companion galaxy as well as from the larger (NELG) galaxy. Thus it is quite likely that X-rays are also emitted from the companion galaxy, thereby accounting for the larger X-ray/optical offset of the NELGs as the optical coordinates given are those of the nucleus of the larger galaxy.

4.3 Identification Content as a function of flux

In figure 8 we show the number of sources in our complete area for the major identification classes, as a function of flux. The dashed line gives the number actually detected and the solid line gives the number corrected for effective area as described above. No correction is applied here for sources lost due to confusion. However such a correction is applied to the calculation of the source count slopes given in Table 5. The only objects not plotted in figure 8 are the 3 definite identifications with stars. Only those sources for which the identification is reasonably firm, ie confidence classes '*' or '(*)', are plotted in specific astrophysical classes (ie QSOS, NELGS, CLUSTERS); the 5 objects of possible but uncertain identification listed in Table 3 are plotted as 'UNIDENTIFIED' together with the blank fields and the two sources whose identification class is given as '?' in Table 3.

4.3.1 QSOs

There are 32 QSOs in our sample and they dominate the bright end of the source counts, but not the faint end. Above 10^{-14} erg cm^{-2} s^{-1} 16 of the 19 sources (ie 84%) in the complete sample are QSOs (the others being 1 NELG, 1 cluster and 1 star). At bright fluxes our results are therefore similar to those of earlier less deep ROSAT observations, eg the 30ksec observation of Shanks *et al.* (1991). In the latter observation 24 of the 39 X-ray sources were identified with QSOs, 5 with stars but with no other class of object being a signficant contributor. However in our survey below $10^{-14.5}$ erg cm^{-2} s^{-1}, only 5 (26%) of the 19 sources are QSOs.

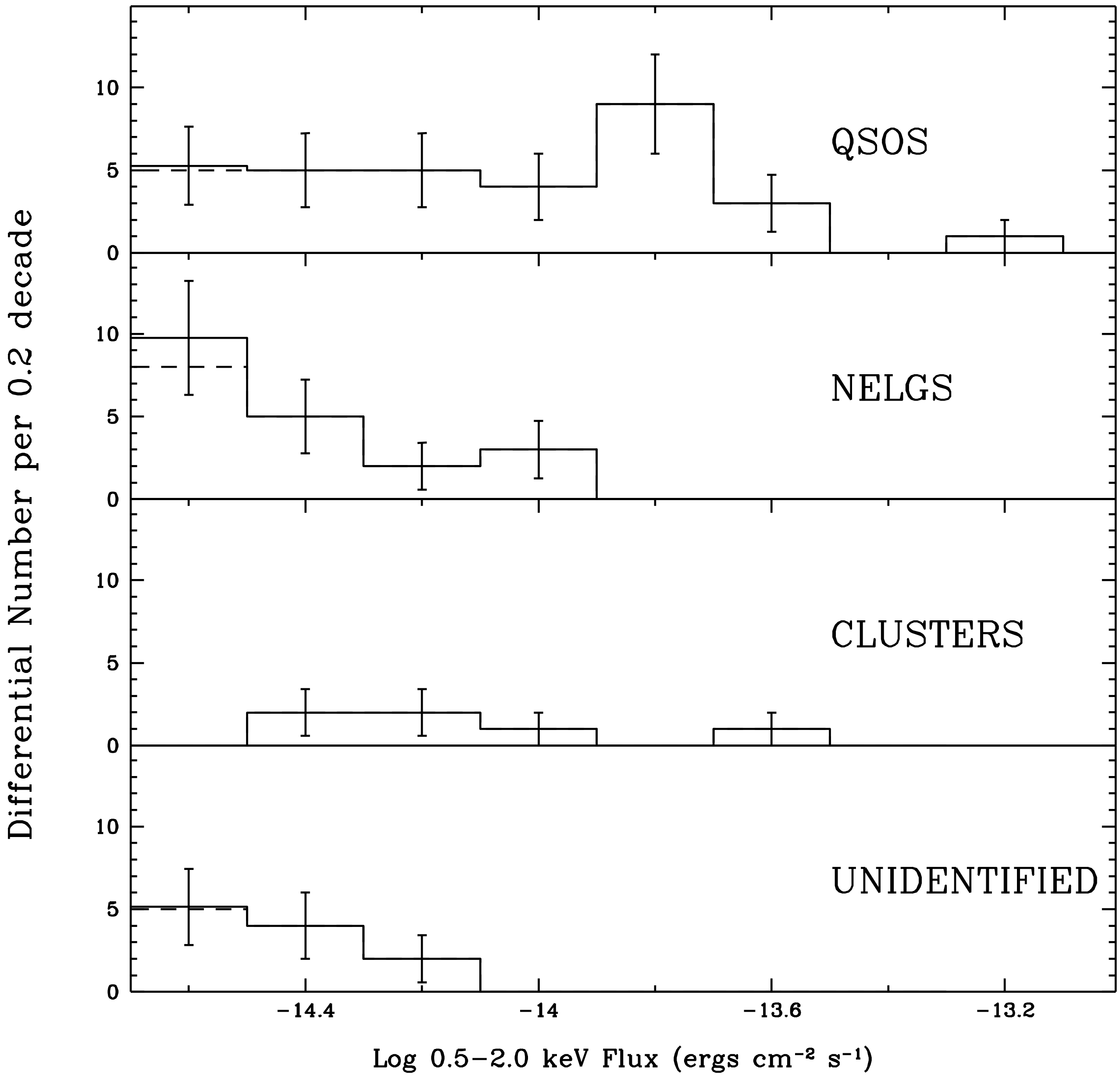

Figure 8. Differential number of QSOs, NELGs, clusters and unidentified sources in the complete area as a function of source flux in 0.2 decade flux bins. The dashed line is the actual number of sources counted; the solid line is the number corrected for the reduction in effective area at low fluxes. No correction is applied here for sources lost due to confusion.

The distribution of our X-ray selected QSOs rises with increasing magnitude to R=21 (3 of R< 19, 5 of R=19-20, 12 of R=20-21). Comparison of surface densities indicates that, at these brighter magnitudes (R< 21), we have probably detected almost all of the QSOs that would have been picked out by optical surveys. In our survey we find a QSO surface density of 129±28 deg^{-2} at R< 21, which corresponds to B$\lesssim$21.5, assuming that the the mean optical QSO colour of B-R≈0.5 (e.g. Boyle, Jones & Shanks 1991) at the redshift of the majority of the QSOs (z<2.9) applies here. The surface densities found in B band optical surveys at the fainter limit of B<22 are slightly less than this value (77±10 deg^{-2} and 115±16 deg^{-2} were found by Boyle, Jones & Shanks (1991) and Zitelli et al. (1992) respectively), suggesting that at R< 21 we are complete. At fainter magnitudes the distribution falls off (10 of R=21-22, 2 of R>22) and so we might ask whether we have missed any faint QSOs.

The obvious answer as to why there are so few QSOs

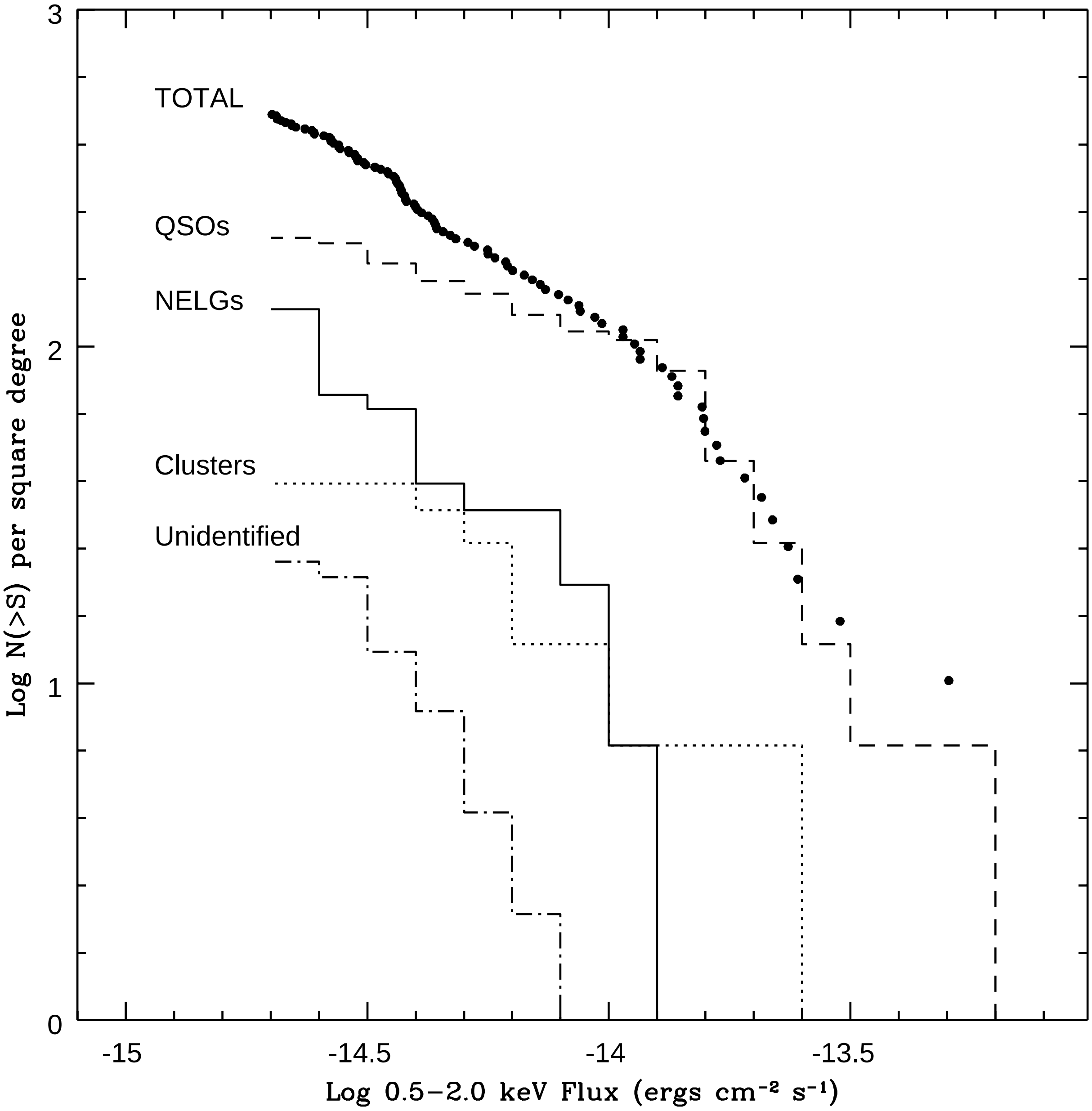

Figure 9. Integral surface density of QSOs (dashed line), NELGs (solid line), clusters (dotted line) and unidentified sources (dot-dash line) from the complete sample, together with the total surface density of sources from the full 15 arcmin radius area (filled dots), as a function of flux. The only identified sources not plotted are the the 3 stars. The numbers are corrected for incompletness of the area at faint fluxes and the unidentified sources are shifted down by 0.5 decade in surface density to avoid overlapping the NELG plot. No correction is applied here for sources lost due to confusion.

of R> 22 is that the X-ray fluxes of any such QSOs would lie below the survey limit. We can crudely address this possibility by reference to the distribution of X-ray fluxes and R-band magnitudes which is given in figure 10. For any given X-ray flux away from the survey limit the range of observed R-band magnitudes is typically 2 magnitudes. However at the survey flux limit the range is somewhat truncated to about 1 magnitude. The optically brightest QSO near the X-ray survey limit has R∼ 21 but the faintest QSO only has R∼ 22. Thus if the X-ray/optical ratio, and dispersion therein, is the same at all fluxes, it is likely that we have missed a few fainter QSOs.

At present the faintest optical survey sensitive to QSOs at all redshifts (as is our X-ray survey) is that of Schade *et al.* (1996) who found 6 QSOs to I_{AB} <22.5 (or B<23) serendipitously in the CFRS survey. The corresponding QSO

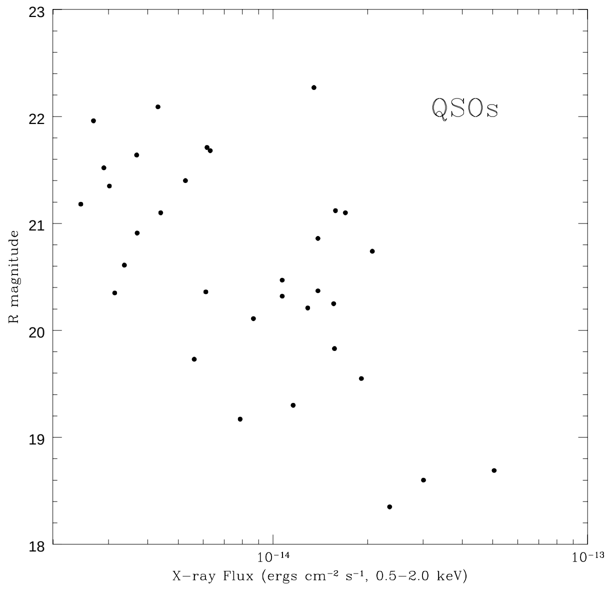

Figure 10. Distribution of X-ray fluxes and R-band magnitudes for the QSOs identified in the present survey. Errorbars are not shown to avoid cluttering the diagram but the X-ray flux errors are given in Table 3 and typical optical errors are 0.1 magnitude, or better.

surface density is 200^{+120}_{-80} deg^{-2}, similar to our value of 210±40 deg^{-2} at R<22, suggesting that we are reasonably complete to at least R=22, in agreement with the distribution shown in figure 10. Although our spectroscopic limit for galaxies is $R \sim 22$, we generally made efforts to obtain spectra of even fainter stellar objects and so we suspect that any missing QSOs have R∼ 23, or fainter. Until we have complete identification of our survey we cannot say how many of such QSOs there may be although we note that 3 of the sources classed as 'unidentified' have objects of R=23 near the centres of the errorboxes, and there are also 4 blank fields. In addition up to 5 of the NELGs may be misidentifications (see next subsection). It is unphysical to suppose that all the unidentified sources will turn out to be QSOs and that there will be no further identifications with optically fainter NELGs or clusters of galaxies (see NELG and QSO source counts in figure 8) however it is quite reasonable that up to half of the uncertain identifications will later turn out to be associated with faint QSOs.

4.3.2 NELGs

NELGs make almost no contribution to our survey above 10^{-14} erg cm^{-2} s^{-1}, but they are the major contributor below $10^{-14.5}$ erg cm^{-2} s^{-1} (where there are 8 NELGs (42%), 5 QSOs, 1 star and 5 unidentified sources). From their rising source counts (see below for details) compared to the flat QSO source counts, we can see that NELGs represent a potentially large contribution to the soft XRB.

Galaxies with narrow emission lines have, of course, been detected as X-ray sources since the earliest days of X-ray astronomy. Most of the early detections of narrow emission line galaxies were of relatively high excitation Seyfert 2 galaxies whereas our NELGs have a mixture of excitations, generally somewhat lower than that of Seyfert 2's. NELGs with similar optical spectra to ours have recently been detected in less deep X-ray surveys, eg EMSS (Stocke *et al.* 1991), Boyle *et al.* (1995), Carballo *et al.* (1995). At brighter fluxes ($> 2 \times 10^{-14}$ erg cm^{-2} s^{-1}) where the QSO source counts are still rising, Boyle *et al.* also find a rising NELG source count. However here we show that, at faint fluxes, whilst the QSO source counts fall, the NELG source counts are still rising.

To determine how many of the NELG identifications are chance associations we assume an average errorbox radius of 10 arcseconds which, as we have shown above, is a somewhat pessimistic figure. We expect 0.25 unrelated galaxies of any spectral type brighter than R=22.0 in each error box (Metcalfe *et al.* 1991) or 0.10 unrelated galaxies brighter than R=21.0. Ignoring the fields in which we have an unambiguous identification with a QSO, cluster or star, we therefore expect 1 galaxy of R≤ 20.0, 3 galaxies of R≤ 21.0 or 7.5 with R≤ 22.0 in the remaining 30 errorboxes. (As not all field galaxies show emission lines like our NELGs (eg Tresse *et al.* 1996) we could reduce these chance coincidences by about 20% but we do not consider that small deviation here.) There are 10 identifications with NELGs having R≤ 20.0, 6 with NELGs having $20 \leq R < 21$ and 2 with NELGs having $R \geq 21$. We therefore conclude that 13 of the 16 NELGs of $R \leq 21$ are real associations. However although the 2 NELGs with $R \geq 21$ are, as far as we can tell, the most likely identifications of their respective sources, the number of NELGs with $R \geq 21$ does not exceed the number of expected chance coincidences. Thus we conclude that 5 of the 18 NELGs are likely to be chance coincidences. We refer readers to the notes on sources for discussion of individual identifications. Note that, as the X-ray/optical ratio of the NELGs varies considerably (see figure 17), we cannot easily correct the NELG source counts (figures 8 and figures 9) to take account of possible incompleteness as a function of optical magnitude and so these figures remain as observed distributions. Similarly we do not correct the derived source count slopes (Table 5) or the contribution of NELGs to the X-ray background (figure 11) although we do make some broad comments in the appropriate sections.

4.3.3 CLUSTERs

There are 6 clusters or groups in our survey within the complete area. These clusters were classified initially on the basis of a visual estimate of an overdensity of close companions relative to the field and so may not all be real physical associations. Subsequently we have obtained more than one similar redshift of galaxies in the putative clusters in sources 58 and 77 (and 74 in mask K). Also two of the clusters (sources 34 and 58) are associated with extended X-ray emission. Thus at least 3 of the 6 possible clusters are real. However, although we always took spectra of the brightest galaxies in the errorboxes, the possibility of AGN-type activity from a fainter nearby galaxy, rather than true diffuse cluster emission, does exist.

Note that there are no isolated absorption line 'galaxies' left as firm identifications in the complete area; the only 'galaxy' left is of uncertain identification and so classed here as 'UNIDENTIFIED'. All other galaxies showing only absorption line spectra lie in what we classify as 'CLUSTERS' (which here includes groups). With one exception the clusters all lie in the mid-flux range of the survey, below 10^{-14} erg cm^{-2} s^{-1} and above $10^{-14.5}$ erg cm^{-2} s^{-1}. Cluster luminosities lie in the range 10^{42} to few $\times 10^{43}$, characteristic of groups or poor clusters locally rather than either rich clusters or individual (non-AGN) elliptical galaxies. We have not yet performed a proper analysis of the richness of the clusters but eye-ball estimates do generally indicate poorer rather than richer clusters.

The 6 clusters correspond to a surface density of 40 deg^{-2} above a flux limit of 2×10^{-15} ergs cm^{-2} s^{-1} . The lower limit on the number of real clusters is 3, as stated above, corresponding to 20 deg^{-2}. The upper limit is harder to determine until we have achieved satisfactory identifications for the unidentified sources but our best guess, based on visual examination of the optical fields, is about 11, corresponding to 73 deg^{-2}. (Note that no correction is made here, or in figure 9, to account for missing objects at fluxes $>2\text{x}10^{-14}$ ergs cm^{-2} s^{-1} which are too rare to be sampled in this pencil beam survey. For clusters the additive correction is +6 clusters deg^{-2}.) The survey flux limit for clusters is only approximate because in general they are extended sources and we have only included the flux within the psf; however only two of the clusters had a measurable extent and thus the approximation should be reasonably accurate. The number of clusters expected has been obtained by integrating the local cluster X-ray luminosity function of Ebeling et al (1997) over redshift (0<z<2) and luminosities $>10^{42}$ erg s^{-1}.

The number predicted assuming no evolution of the cluster luminosity function and $q_\circ$=0.5 is 22 deg^{-2} (or 32 deg^{-2} for $q_\circ$=0). Thus the number observed is consistent with a no-evolution model, or is possibly slightly higher (ie weak positive evolution). Since 5 of the 6 clusters have measured redshifts of z>0.3, this result implies that the low luminosity clusters observed here do not evolve at the same (negative) rate as that claimed for the high luminosity EMSS ($\sim 10^{45}$ erg s^{-1}) clusters by Henry *et al.* (1992) in approximately the same redshift range. However our results may be consistent with the results of Henry *et al.* as the latter provide no strong evidence for evolution of the lowest luminosity clusters ($\sim 10^{44}$ erg s^{-1}) in the EMSS sample. Strong negative evolution had earlier been claimed for more nearby ($z \leq 0.2$) high luminosity clusters by Edge *et al.* (1990) but Ebeling *et al.* (1997), from ROSAT all sky survey observations, strongly dispute that result. From observations of extended sources found serendipidously in ROSAT pointed observations, Castander *et al.* (1995) found few clusters, again supporting negative evolution, however Collins *et al.* (1997) and Scharf *et al.* (1997), searching the same database, dispute the Castander *et al.* result and find little evidence for any evolution. The Collins *et al.* sample covers the same redshift range as our clusters (z>0.3) and the clusters are of generally intermediate luminosity ($\leq 10^{44}$ erg s^{-1}).

Thus our observations support the growing concensus that there is little evidence for evolution in low luminosity clusters even at quite high redshifts ($z \sim 0.5$); so far only the Henry *et al.* observations sample high luminosities at high redshifts. The detailed implications of our results for models of the growth of structure in the Universe will be investigated in a future paper.

We note that some current cluster surveys (eg Collins *et al.*) rely on detecting extended sources in many separate ROSAT observations. Thus differences in source detection algorithm may affect the number of clusters found, particularly for marginally resolved clusters. However in the present survey, which strives to classify all sources in a selected area, source extension is not the only characteristic used in classification. Supporting optical information is used too. Thus low luminosity, very distant clusters, which may not appear resolved in the X-ray data, are not selected against. With regard to the optical information we note that our clusters are all relatively distant ($z > 0.3$) and even the brightest cluster members are not that bright (typically $m \geq 19$). Some of the clusters which are quite obvious on the 8K×8K images were not at all obvious on our earlier CCD images. It is possible that other surveys with less deep optical imaging may miss distant clusters and it is not impossible that we may find even more, very distant, clusters by the time we have identified all the sources in our complete area.

4.3.4 STARs

There are only 3 definite identifications with stars in our complete sample. One of these, a 13.79 mag M star, happens to be the brightest source in the 15 arcmin field by a factor of ~ 10 over the second source. The two other stars are also late type stars; source 64 is a 13.41 mag G star and source 115 is a 20.23 mag M star. The implied X-ray/optical ratios are typical of coronal emission and similar to the ratios found by Stocke *et al.* 1991 for stars of the same class.

4.3.5 UNIDENTIFIED SOURCES AND BLANK FIELDS

Eleven sources in the complete sample as classified as 'unidentified'. These sources do not occur in the upper third of Table 3, but otherwise are distributed more or less evenly throughout the lower flux range. Of these, seven errorboxes contain objects such as faint galaxies or stellar objects which could be the identification. In some cases (49, 60, 80) there is only one reasonable candidate, each one lying close to the errorbox centre, but the optical spectra are inconclusive. Given the accuracy of our X-ray positions these candidates must be considered fairly likely identifications. In the other 4 cases there is more than one optical candidate and the spectra are again either inconclusive or not available. For 5 of the 7 we make a tentative best guess at the identification class, finding 1 QSO, 1 NELG, 1 cluster, 1 star and 1 absorption line galaxy. We refer to the notes on individual objects for more information.

In 4 cases we find no objects brighter than ~ 23mag in the errorboxes. Some of these 'blank' fields contain even fainter objects in the errorbox, but nothing more than one would expect by chance at such magnitudes. Given the accuracy of our X-ray positions (figure 4) we are confident that the positions of these blank fields are good and so we must ask what the identifications could be. Possibilities include very distant clusters or highly reddened AGN but we can draw no further conclusions on the basis of the present data.

Table 4. IDENTIFICATION SUMMARY

	BRIGHT $> 10^{-14}$	FAINT $\leq 10^{-14.5}$ erg cm^{-2} s^{-1}	ALL
QSOs	16	5	32
NELGs	1	8	18
Clusters	1	0	6
Stars	1	1	3
Unidentified	0	5	11

The results of deep infrared imaging are reported elsewhere (Newsam *et al.* 1997).

4.4 Source Count Slopes

We can see from figure 8 that the number of QSOs per logarithmic flux bin is constant below 10^{-14} erg cm^{-2} s^{-1} whereas the number of NELGs per logarithmic flux bin is increasing. In order to quantify this effect we have performed a maximum likelihood fit to find the best single power-law slope to the distribution of sources. We perform the fit over the flux range 2×10^{-15} erg cm^{-2} s^{-1} to 1×10^{-14} erg cm^{-2} s^{-1}. For the NELGs the choice of upper flux limit does not affect significantly the derived slope but the error increases as the flux range is reduced. For example taking an upper flux cut off of $10^{-13.6}$ erg cm^{-2} s^{-1} gives a slope of $-2.37^{+0.32}_{-0.58}$ (uncorrected) or $-2.44^{+0.33}_{-0.56}$ (corrected). However for the QSOs the choice of upper flux limit does affect the derived value as the QSO source counts steepen above 1×10^{-14} erg cm^{-2} s^{-1}. As we are interested in the most realistic extrapolation of the source counts to fluxes below our survey limit, we restrict our fitting to the sources of flux below 10^{-14} erg cm^{-2} s^{-1}. The best fit slopes to the differential source counts are given in Table 5.

As already stated in section 4.3.2, we have not attempted to correct the NELG source count slopes for chance associations as we do not know which these are. However of the 8 NELGs with R$\geq$ 20, of which 4 are expected to be chance coincidences, 5 have X-ray fluxes $< 2.25 \times 10^{-15}$ erg cm^{-2} s^{-1}, ie just above our survey limit. Thus removal of chance coincidences will probably flatten the NELG source counts. However, as we have 11 sources classed as 'unidentified', whose source counts rise at a similar rate to that of the NELGs, it is quite possible that new NELGs may be discovered to compensate for the chance associations. Given these uncertainties we do not alter the observed distributions.

Although not plotted in figure 9, the integral source count slope derived from the 12 NELGs in the Boyle *et al.* (1995; CRSS) survey at fluxes $> 10^{-14}$ erg cm^{-2} s^{-1} does join on quite smoothly to the present NELG source count slope at fainter fluxes. It is not certain that the CRSS NELGs are exactly the same sort of animal as our present NELGs (eg the CRSS NELGs are slightly more luminous, $10^{42} < L_X < 10^{43}$ ergs s^{-1}), but their optical spectra are rather similar. We have therefore calculated the maxiumum likelihood source count slope for the combination of the 18 NELGs from the present deep survey and the 12 CRSS NELGs. We perform the fit over the flux range 2×10^{-15} erg cm^{-2} s^{-1} to 1×10^{-13} erg cm^{-2} s^{-1} and the fit is given at the bottom of Table 5. The combined fit is quite consistent with the fit based solely on the present deep survey NELGs, and is consistent with a Euclidean slope. The error on the combined slope is, of course, less than on the slope of the deep survey NELGs alone.

On the basis of these data, the NELG source counts are quite consistent with a Euclidean distribution but the QSOs source counts definitely are not and imply that we are seeing beyond a cut-off in the redshift distribution of X-ray QSOs. We noted, in section 2.1.2, that the faint end source count slope for all sources in the complete area are slightly flatter (although only at the 1σ level) than those in the full 12 arcmin or 15 arcmin radius X-ray survey area. We repeat the complete area slopes in Table 5 as those are the ones we should compare the QSO and NELG counts with. In Section 6 we use these slopes to extrapolate the contribution of various classes of objects to the soft XRB to flux limits below that of the present survey.

5 X-RAY SPECTRA

Ideally any major contributor to the XRB should have a similarly hard spectrum. The 0.1-2.0 keV spectrum of that part of the X-ray background which remains unresolved in the deepest ROSAT observations is best fit (GBR), assuming an obscuring column at the galactic value, by a combination of a very cool (kT=0.1 keV) thermal bremsstrahlung component and a power-law of energy index 0.7 which dominates above 0.4 keV. Recent ASCA observations (Gendreau *et al.* 1995) indicate that the XRB spectrum may be even harder ($\alpha \sim 0.4$ in the 1-10 keV range).

The work of GBR and others (eg Romero-Colmenero *et al.* 1996) confirms that the X-ray spectra of QSOs in the ROSAT band, $\alpha \sim 1$, are steeper than the spectrum of the diffuse XRB within the ROSAT band. If the QSO spectra extrapolate to higher energies then they cannot contribute all of the high energy XRB. In Table 3 we present the hardness ratios of the brighter ROSAT sources. The hardness ratio is defined as the ratio of counts in the 0.5-2.0 keV band to those in the 0.1-0.5 keV band. For those sources which were undetected in the soft (0.1-0.5 keV) band we assume a soft count rate equal to that of the faintest source detected in the soft band. The counts in the soft and hard bands were derived by psf fitting to images made in those bands rather than by simply counting photons within a certain radius of the X-ray centroid. Thus they should be reasonably robust to the presence of nearby sources. However when a particularly soft source (eg 15) is very close to a particularly hard one (source 2), the hard source may then not be detected at all in the soft band and so the hardness ratio of the hard source may be overestimated. Thus, although the hardness ratios do not contain as much spectral information as a proper spectral fit, they do provide a reasonable description of the X-ray spectra. The hardness ratios cease to be useful below about source 80 where the lower limits on the source hardness can only be used to eliminate sources with extremely soft spectral indices.

In Table 6 we give the hardness ratios expected from various spectral models. We can see that the hardness ratios actually provide a remarkably good diagnostic of spectral type. For example, power law models (assuming a galactic absorbing column), unless noticeably flatter than $\alpha = 1$, are readily distinguished from Raymond-Smith thermal models.

Table 5. QSO AND NELG DIFFERENTIAL SOURCE COUNT SLOPES AT FAINT FLUXES

	All Sources	QSOs	NELGS
Uncorrected	$-1.42^{+0.19}_{-0.26}$	$-1.26^{+0.50}_{-0.55}$	$-2.06^{+0.50}_{-0.58}$
Corrected for Confusion	$-1.53^{+0.19}_{-0.28}$	$-1.40^{+0.48}_{-0.61}$	$-2.23^{+0.53}_{-0.63}$
Corrected for Missing Area and Confusion	$-1.46^{+0.19}_{-0.28}$	$-1.33^{+0.53}_{-0.55}$	$-2.15^{+0.50}_{-0.65}$
Including 12 CRSS NELGs to flux 1×10^{-13} erg cm^{-2} s^{-1}			$-2.46^{+0.14}_{-0.17}$

For the Raymond-Smith thermal models we also note that the gas temperature does not have a great effect on the hardness ratio. However the metallicity is very important because of the dominant iron-L emission at ~1 keV. Thus high metallicity thermal sources (eg stars) can, in general, be distinguished from low metallicity thermal sources such as clusters of galaxies.

Examination of Table 3 shows that the NELGs are, on average, significantly harder than the QSOs. For example, taking an arbitrary hardness ratio of 0.8, we can see that all NELGs brighter than source 60 have hardness ratio above 0.8. (Below source 60 the lower limit on the hardness ratio for sources undetected in the soft band is generally below 0.8). However only a few of the QSOs are harder than 0.8 and these include sources 2 and 24 which are not detected in the soft band because of the presence of a very soft nearby confusing sources (15 and 20 respectively). Unfortunately there are insufficient photons to simultaneously provide useful constraints on both the power-law index and the absorbing column but a fit to the summed spectra of the 5 brightest NELGs shows no evidence of strong absorption, ie the column is $2.2^{+2.6}_{-1.8} \times 10^{20}$ cm^{-2} and the energy index is $1.06^{+0.7}_{-0.6}$. Examination of the spectra of individual bright NELGs indicates possible differences in absorbing column between individual NELGs but the sources are too faint for definite statements to be made. The above hardness ratio results were noted by M^{c}Hardy (1995). Carballo *et al.* (1995) also calculated hardness ratios for the sources in their sample and concluded that galaxies without broad emission lines had very hard spectra. A more detailed X-ray spectral analysis of the galaxies in the present sample was then presented by Romero-Colmenero *et al.* (1996). Romero-Colmenero *et al.* found that the average NELG spectral index, $<\alpha>= 0.45 \pm 0.09$ (assuming a galactic absorbing column) whilst that of the QSOs is 0.96 ± 0.03. Thus the average spectrum of the NELGs is in good agreement with the background spectrum and is certainly a better fit to it than is the average QSO spectrum. A similar result was subsequently found by Almaini *et al.* (1996) from examination of a somewhat X-ray brighter sample of NELGs. Almaini *et al.* also conclude that the average absorbing column of the NELGs is close to the galactic value but do find some sources with higher than galactic absorbing columns.

An X-ray spectrum without observable absorption can, of course, be produced by scattering even though all direct low-energy emission might be completely absorbed. A column density of $\sim 5 \times 10^{23}$ atoms cm^{-2} would be sufficient to prevent direct radiation from the brightest known (2-10 keV) AGN being detected in our ROSAT observations. However if we were seeing scattered, rather than direct, X-radiation from our NELGs, then their implied luminosities at energies >10 keV would be very large $> 10^{45}$ ergs cm^{-2} s^{-1} (eg see ASCA and OSSE observations of NGC4945 by Done *et al.* 1996) and the integrated emission from all NELGs would greatly exceed the observed hard X-ray background.

Table 6. HARDNESS RATIOS FOR SPECTRAL MODELS

HR	$<E>$(keV)	Model
0.13	0.3	PL with $\alpha = 2$
0.5	0.5	PL with $\alpha = 1$
0.9	0.6	1 keV RS model (Z=0.3)
0.94	0.65	5 keV RS model (Z=0.3)
1.7	0.7	1 keV RS model (Z=1)

Table 7. NELG PERCENTAGE CONTRIBUTION TO THE HARD X-RAY BACKGROUND

Lower flux Limit (ergs cm^{-2} s^{-1}, 0.5-2 keV)	5 keV	10 keV	20 keV
2×10^{-15}	10.0 (7.8)	10.2 (7.9)	11.6 (9.0)
5×10^{-16}	20.6 (23.7)	20.8 (23.9)	23.8 (27.3)

Taking the X-ray spectral index of the NELGs to be 0.45, and taking the differential source count slope to be -2.2 we can calculate the contribution of NELGs to the X-ray background at any arbitrary energy. The only variable is then the lower flux limit in the ROSAT band at which one cuts off the contribution of NELGs. For the X-ray background spectrum at energy, E, in the energy range 3 to 60 keV, we use the expression of D E Gruber, given in Fabian and Barcons (1992, equation 2) as:

$$I(E) = 7.877E^{-0.29}exp(-E/41.13)keVs^{-1}sr^{-1}cm^{-2}keV^{-1}$$

The resultant percentage contributions at energies of 5, 10 and 20 keV are given in Table 7. The percentages in brackets are those applicable to a differential source count slope of -2.5.

If we ignore all other possible contributors to the hard X-ray background then Table 7 directly gives us the lower limit to the fraction of the NELG X-ray emission which we can allow to be scattered if we are not to exceed the total X-ray background flux. Thus if the scattering model is to succeed we require a scattering percentage of at least 10%, and probably greater than 20%, which is a much higher percentage than the ball park figure of $\sim 1\%$ which is usually assumed. Including contributions to the hard X-ray background from other sources such as clusters and Seyfert galaxies which we already know to exist only raises the lower limit to the allowed scattering fraction.

Moreover high fluxes in the hard X-ray band are likely to be associated with high optical fluxes, ie bright galaxies (eg see Elvis *et al.* 1978), and we note that NGC4945 is a 9th magnitude galaxy whereas our NELGs are 18-21 mag. Scattering might also be expected to produce weak broad bases to the permitted lines. However, with the exception of object 51 where no such broad bases are seen, the present optical spectra are not good enough to put useful limits on the strength of any possible broad lines. We conclude that it is much more likely that we are looking at direct, rather than scattered, radiation from the NELGs and so the majority of them probably do have low intrinsic absorbing columns.

A number of other points related to the identification content of the survey can be made from examination of the hardness ratios. It is quite clear that there is a wide range in the X-ray spectra of the QSOs. Some are extremely soft with implied power-law energy indices steeper than 2. Only the QSOs have such soft spectra. We may therefore conclude that the unidentified source 9, which also has a very soft spectrum, is probably also a QSO and, conversely, the unidentified hard source 54 is more likely to be a NELG than a QSO, although we do note that there are some quite hard QSOs. On the basis of the hardness ratio alone we cannot rule out the possibility that a high hardness ratio in a QSO is a result of absorption although, with few exceptions, X-ray selected QSOs are rarely highly absorbed.

With the exception of source 5, which is slightly confused, all the proposed cluster identifications have relatively high hardness ratios, consistent with what we expect from a low metallicity hot gas. Thus we strengthen our belief in the majority of cluster identifications and confirm our suspicion, based on examination of the X-ray and optical fields, that source 5 may contain emission from more than one discrete location.

With the exception of the rather unusual emission line M star, source 1, the other stellar identifications, 16 (M star) and 27 (G star), have high hardness ratios (1.44 and 1.20 respectively) entirely consistent with high metallicity thermal plasma emission.

Thus a rather consistent pattern emerges between the identifications and their X-ray spectra, further strengthening our confidence in the identifications and providing some grounds for guessing at what at least the brighter of the presently unidentified sources might be.

6 CONTRIBUTION OF THE IDENTIFIED SOURCES TO THE SOFT X-RAY BACKGROUND

In figure 11 and Table 8 we present an estimate of the contribution of various classes of object to the diffuse 1-2 keV XRB, above a particular flux, based on their differential source counts, corrected for missing area and confusion losses. The source counts have been extrapolated down to 2×10^{-16} ergs cm^{-2} s^{-1} (0.5-2 keV) at which point almost all of the soft XRB would be accounted for. For the QSOs and NELGs we plot the best fit prediction as thick lines (solid for the NELGs, dot-dash for the QSOs) and also plot 1σ error bounds as thin lines. The upper uncertainty bound for the NELGs is particularly large and identification of X-ray sources only a little fainter than the limits of our present X-ray survey would greatly reduce the uncertainty. Similarly, inclusion of NELGs with brighter fluxes would also reduce the uncertainty. We have earlier calculated the NELG source count slope from a combination of our present NELGs and the 12 CRSS NELGs. To avoid confusion we do not add further lines to figure 11 but we note that the steeper combined NELG source counts predict a contribution to the soft XRB somewhat in excess of the best fit shown in figure 11 (ie around 30% at 2×10^{-16} ergs cm^{-2} s^{-1}). However the reduced error on the combined slope means that the upper bound is consequently reduced (to around 40% at the same flux level).

As stated in section 6, removal of NELG chance coincidences will probably flatten the NELG source counts and so reduce the contribution of NELGs to the soft XRB at faint fluxes. However the uncertainties associated with NELG chance associations, and with any NELGs which may not yet be identified, prevent us from making any quantitative correction. Of course a smooth extrapolation to 2×10^{-16} ergs cm^{-2} s^{-1} followed by a sharp cut-off is unrealistic and so it is likely, for example, that the NELG source counts will turn down at some flux limit below our survey limit. However as yet we have no evidence as to what that flux limit might be. We remind reader that the unidentified sources provide a major uncertainty in determining the origin of the XRB. We have already argued (section 4.3.1) that some unidentified sources will be faint QSOs and so we underestimate the contribution of QSOs to the soft XRB. However as it is impossible to estimate precise numbers, we do not attempt any correction to the QSO contribution. It is therefore unrealistic to extrapolate the unidentified sources as if they were a uniform class of objects. Despite these provisos, figure 11 does provide a first order prediction which future deeper surveys can address.

In Table 8 we also list the contribution to the 1-2 keV XRB from resolved sources in various flux ranges higher than those covered by our own survey. These higher flux contributions are also included in figure 11. This source-count based approach clarifies the contribution of various classes to the XRB in particular flux ranges and allows simple extrapolation to fainter fluxes (although, of course, such extrapolations should not be pushed too far). Also it is simple to take into account possibilities such as all of the unidentified sources being NELGs.

To avoid contamination of the extragalactic XRB by diffuse soft emission from our own galaxy we follow previous workers (Hasinger *et al.* 1993) and restrict discussion to energies above 1 keV. We assume a 1-2 keV X-ray background intensity of 1.46×10^{-8} erg cm^{-2} s^{-1} sr^{-1} (Chen, Fabian & Gendreau 1996), which is consistent with the value of 1.4×10^{-8} erg cm^{-2} s^{-1} sr^{-1} found by GBR. Fluxes have been converted to the 1-2 keV band assuming an energy index of 1 for the QSOs, 0.45 for the NELGs and clusters and 0.7 for the unidentified sources, and a column density $N_H = 6.5 \times 10^{19}$ cm^{-2}.

As is already clear from figures 8 and 9, we see again in Table 8 and figure 11 that QSOs are the dominant contributor to the 1-2 keV XRB at bright fluxes whereas NELGs dominate at low fluxes. By extrapolating the differential source counts to fluxes below our survey limit we see, in Table 8, that QSOs contribute very little more to the soft XRB whereas the contribution from NELGs continues to rise. Indeed, if the NELG source counts continue to rise then the overall source counts should start to show an upturn at

Table 8. 1-2 KEV X-RAY BACKGROUND PERCENTAGES AS A FUNCTION OF FLUX

Flux erg cm^{-2} s^{-1} (0.5-2 keV)	1x10^{-11} -5x10^{-14}	1-5 x10^{-14}	2-10 x10^{-15}	Total to 2x10^{-15}	0.5-2x10^{-15} Extrapolation
All extragalactic	11[†]	23[‡]	18[♯]	52	$\sim$ 18
QSOs	7[♭]	18[‡]	6[♯]	31	2
NELGs	<0.7[§]	$\sim$1[⊕]	6[♯]	$\sim$ 8	9
Clusters	1.4[◇]	5.5[◇]	3[♯]	10	0.5
Unidentified			3[♯]	3	6

† From the model fit to the extragalactic Einstein Medium Sensitivity Survey (EMSS) of Gioia *et al.* (1990a).
‡ From Shanks *et al.* (1991), Table 3.
♯ Present work.
♭ From EMSS AGN data (Maccacaro *et al.* 1991).
§ From EMSS data (Stocke *et al.* 1991). This is an upper limit since it includes all EMSS galaxies which may have narrow lines.
⊕ Estimate from the 12 NELGs in 5 ROSAT fields found by Boyle *et al.* (1995).
◇ From Jones *et al.* , in preparation.

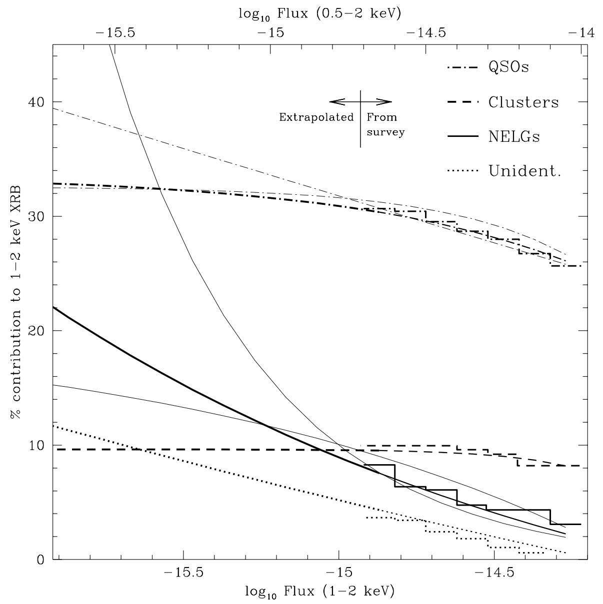

Figure 11. Contribution to the 1-2 keV X-ray background from sources of different types, above a given flux. Below our survey limit the extrapolations are based on maximum likelihood fits to the corrected differential source counts given in figure 8. The flux ranges over which the source count slopes were calculated are given in the text. For the NELGs and for the QSOs we present 1σ confidence limits in the form of thinner lines of the same type (ie solid for the NELGs, dot-dash for the QSOs).

fluxes not far below our survey limit. Although not required by the ROSAT deep field fluctuation analyses (Hasinger *et al.* 1993; Barcons *et al.* 1994) the predicted upturn is consistent with these analyses. A useful constraint on NELG evolution would therefore be provided by a survey which extended the soft X-ray overall source counts, without the need for identifications, to a flux limit a factor of only a few below the present survey limit.

In Table 8 we separately list the contribution to the soft XRB of the unidentified sources. The unidentified sources have a rising source count slope similar to that of the NELGs and some unidentified sources are very probably NELGs, but obscured QSOs or very distant clusters cannot be ruled out at this stage. The unidentified sources provide the major uncertainty in the contribution of the various identified classes of sources to the XRB and so completion of the identifications of our sample remains a high priority.

An estimate of the contribution of various classes of object to the XRB can also be made by modelling the evolution of their luminosity functions. The evolution of the QSOs in the present sample, together with QSOs from the EMSS sample (Stocke *et al.* 1991), has been considered by Jones *et al.* (1997) and, considering also RIXOS and other samples, by Page *et al.* (1997a). The evolution of the NELGs in the present sample has been considered by Page etal (1997b) and Pearson *et al.* (1997). Jones *et al.* deduce that, depending on the evolutionary model chosen, between 31% and 51% of the soft XRB can be contributed by QSOs and Page *et al.* (1997b) agree, giving an upper limit of 45%. The present QSO results are in agreement with the previous work although towards the lower end of the Jones *et al.* range. Page *et al.* (1997b) conclude that NELGs contribute between 15% and 35% of the soft XRB, in approximate agreement with extrapolations from previous surveys eg Boyle *et al.* (1995). Our NELG results are also in agreement with previous work.

We have resolved a total of 52% of the 1-2 keV X-ray background into point sources at the flux limit of 2x10^{-15} erg cm^{-2} s^{-1}. Most of the resolved flux (31%) arises from QSOs. Approximately 8% arises from NELGs, and the rest comes from clusters and groups of galaxies ($\sim$ 10%), with some sources as yet unidentified. However extrapolating the differential source counts to a flux a factor 4 below the survey limit (5×10^{-16} ergs cm^{-2} s^{-1}), we expect that $\sim$ 70% of the 1-2 keV XRB would be resolved. The NELG surface density at 5×10^{-16} ergs cm^{-2} s^{-1} would be between 1000 and 2500 deg^{-2} sufficient, unlike the surface density of QSOs, to explain the isotropy of the XRB (see Fabian and Barcons (1992) for a review of the isotropy of the XRB).

6.1 Implications for the Hard X-ray Background

The NELGs have hard X-ray spectra, similar to that of the XRB, and harder than those of Seyfert galaxies in the 2-10 keV range ($<\alpha>\sim 0.8$). If their X-ray spectra extrapolate smoothly to higher energies (see section 7) they will be significant contributors to the XRB at energies above those considered in the present survey ($0.5-2$ keV). As their spectra are similar to the XRB then, to first order, they will contribute similar fractions of the XRB in higher energy bands as they do in the ROSAT band (Table 7). Thus they will be significant contributors but, assuming that we can ignore the scattering model for their X-ray spectra discussed in section 5, they will not explain all of the presently unresolved hard XRB and, as in every new band, new populations of sources will be needed. However, as in the present study, NELGs will only be detectable as significant contributors at faint fluxes, well below the level of all sky surveys such as that of Ariel V (M^{c}Hardy *et al.* 1981). NELGs should be detectable in small numbers in deep ASCA observations but in large numbers in XMM and AXAF observations.

7 NELGS - AGN OR STARBURST GALAXIES?

To determine what the NELGs might be, and how they might relate to other established galaxy types, we consider next their photometric and spectroscopic properties.

We have observed the majority of the survey field in the V-band as well as R-band, and some I-band observations have also been made. Thus we have observed V-R colours for the NELGs. These colours, which correspond to approximately rest frame B-V colours, or even bluer in most cases, lie in the range 0.1-1.0, with a mean around 0.5, more indicative of spiral than elliptical galaxies.

Morphologically, we have obvious visual examples of spiral host galaxies in the more nearby NELGs (eg source 32). We also note that some galaxies appear flattened (eg ROSAT 93 and 103) whilst others are more circular (ROSAT 121). Thus some NELGs are certainly spiral galaxies, but the possibility that some are elliptical galaxies cannot be ruled out at this stage. We also note some rather distorted morphologies and evidence of interactions with neighbouring galaxies in many cases. The results of visual examination are given in the notes on individual sources. However a proper morphological classification of the majority of NELGs on the basis of our present CCD data requires model fitting. A proper morphological and colour analysis of the NELGs will be presented in a future paper (Newsam *et al.* , in preparation).

The observed NELGs lie in the redshift range 0.061 to 0.590, with the majority lying in the range 0.2-0.4. Within the present small sample there is no evidence for evolution in the NELG population or for a redshift cut-off, principally because of the uncertainty associated with the nature of the unidentified sources. However when the present sample are combined with NELGs from the RIXOS sample, there is some evidence for evolution (Page *et al.* 1997b), but at a slower rate than found for broad line AGN. From analysis of a small sample of NELGs with brighter fluxes, Boyle *et al.* (1995) find a broadly similar result to that of Page *et al.* . Griffiths *et al.* (1996) claim a higher rate of NELG evolution but their sample consists of NELGs from both ROSAT and Einstein observations and so may be subject to additional uncertainties. The details of NELG evolution are therefore far from clear and even deeper X-ray surveys are required to resolve the isssue.

The absolute magnitudes of the NELGs lie in the range M_R -20 to -23, typical of large spirals or ellipticals. However their X-ray luminosities lie in the range 3×10^{41} to 5×10^{42} ergs s^{-1}, factors of 10-100 more than normal large spiral galaxies and at the upper bound for large non-cluster ellipticals (see Fabbiano 1989 for a review of X-ray emission from normal galaxies). AGN can easily produce such X-ray luminosities, which are towards the lower end of the distribution of AGN X-ray luminosities. However typical AGN X-ray spectra are steeper (energy index ~ 0.8) than the observed average NELG X-ray spectral index ($\sim$ 0.45). Blazar-like AGN (eg 3C273, Turner *et al.* 1990; Leach *et al.* 1995) have similarly flat X-ray spectra but have much higher observed luminosities ($\geq 10^{45}$ ergs s^{-1}). Recently there has been some interest in advection dominated accretion onto black holes (eg Narayan and Yi 1995). Such accretion produces a very hard X-ray spectrum and so advection dominated accretion onto a very massive black hole could account for both the observed luminosities and X-ray spectra of the NELGs.

X-ray data on starbursts galaxies is not as good as for AGN because of the generally lower X-ray fluxes of starburst galaxies. Many 'starburst' galaxies of apparent high X-ray luminosity turn out, on closer inspection, to be AGN (eg Moran *et al.* 1994). The maximum luminosity so far detected (0.5-2 keV) is $\sim 2 \times 10^{41}$ ergs s^{-1}; Griffiths and Padovani 1990; Read and Ponman 1997). However with these provisos we note that Rephaeli *et al.* (1995) measure the average X-ray spectral index of 51 candidate starburst galaxies to be 0.47 ± 0.26 (1-100 keV), very similar to the average spectral index of the NELGs. Rephaeli *et al.* also consider various possible X-ray emission mechanisms. They conclude, as does Fabbiano (1989), that X-ray binary sources, which have hard X-ray spectra extending out to at least 20 keV, can contribute up to 10^{41} ergs s^{-1}. Such binary systems, which would be distributed throughout the bulge and disc, would be resolvable in many of our NELGs by AXAF. Other possibilites include supernovae remnants (which have a variety of spectral indices), Compton scattering off relativistic electrons from supernovae (hard spectrum) and thermal emission from a supernova-driven galactic wind or from an extended gaseous halo (soft spectrum). These possibilities require high supernovae rates.

A simple scenario is that starburst/X-ray binary activity dominates the X-ray emission from the lower luminosity NELGs but that AGN activity dominates the higher luminosity ones. More detailed observations, particularly X-ray spectral observations of individual NELGs such as will be possible with XMM, are required to clarify the issue.

Our optical spectra (figures 12, 13 and 14) show a variety of narrow (FWHM $<$ 1000 km/s) emission lines. H_α is often redshifted out of the detectable spectral band but [OII] is usually within range, and present. The rest frame equivalent width of [OII] is typically 20-60Å, larger than that found in nearby galaxies except for irregular galaxies and Markarian galaxies (Kennicutt 1992). H_β and [OIII] are usually in range and sometimes present. Although the spectra are not all of the same signal to noise, it is clear that the spectra are not all identical. Some show strong lines, others weak, and the line ratios vary between the spectra.

In order to quantify the spectra we have plotted the standard diagnostic line ratios (cf Veilleux and Osterbrock 1987) of [OIII]5007/H$_\beta$ *vs.* [NII]6583/H$_\alpha$ (figure 15), and [OIII]5007/H$_\beta$ *vs.* [SII]6716+6731/H$_\alpha$ (figure 16). Veilleux and Osterbrock show that these line ratios provide a reasonable discriminant between starburst galaxies and true AGN. We find that the NELGs are distributed between the higher ionisation bound of HII region (ie starburst) galaxies and the lower ionisation area of true AGN. Although not plotted here, a further diagnostic diagram is provided by the ratio of [OIII]5007 to [OII]3727 (eg plotted as [OIII]5007/H$_\beta$ *vs.* [OII]3727/H$_\beta$ by Tresse *et al.* (1996) in their figure 3). For our sample [OIII]5007/H$_\beta$ is usually slightly greater than unity and [OII]3727/H$_\beta$ is a factor of a few greater than unity, placing our NELGs in the region of parameter space occupied by LINERs (low ionisation nuclear emission region galaxies, eg Ferland and Netzer 1983). Thus, the NELGs appear to be a mix of galaxy types, generally of low ionisation, including LINERs and starbursts but also some Seyfert II galaxies.

As a further diagnostic of the NELG emission mechanism we plot, in figure 17, the NELG X-ray/optical ratios. Typically accretion powered objects, ie AGN, have X-ray/optical ratios close to unity, whereas starburst galaxies have ratios nearer 10^{-3} (eg Moorwood 1996). Our NELGs have a wide range of ratios and are distributed in between these two values. Taken together with the line ratio plots, the X-ray/optical ratios indicate that there is probably not one single emission mechanism which is responsible for the X-ray emission in the NELGs. It is more likely that there is a mixture of emission mechanisms not only within the sample as a whole but within individual objects. It is likely that both starburst and true AGN emission exists together in many of the NELGs.

In addition to the X-ray and optical surveys, we have carried out deep radio observations of the whole 30 arcmin diameter X-ray survey area with the Very Large Array (VLA) reaching source detection limits of ~ 0.3 mJy at both 20 and 6 cm. A full analysis of these data will be presented elsewhere and here we simply note that, of the 10 X-ray brightest NELGs, 4 are detected in our 20cm VLA survey with fluxes >0.5 mJy. These are noted in Table 3. The luminosities are high ($\sim 10^{23}$ W Hz^{-1} at 20 cm) by normal spiral galaxy standards (Condon 1992) but, with one exception, well below those of classical radio galaxies. Condon shows that radio emission in non-AGN galaxies is related to the recent star formation rate; similarly Benn *et al.* (1993) find that the optical spectra of sub-mJy radio sources are similar to those of the faint starburst galaxies detected in observations with the Infrared Astronomical Satellite Observatory (IRAS). Our radio observations are therefore consistent with the suggestion above that some of the NELG X-ray emission arises in starburst activity.

Some galaxies with similar optical spectra to our NELGs have been detected in previous X-ray surveys with brighter flux limits (eg Boller *et al.* 1993; Boyle *et al.* 1995; Carballo *et al.* 1995). However in these surveys they represented a small fraction of the identified sources. It was therefore not possible to determine reliably whether they were likely to be a major contributor to the XRB at fainter fluxes or not. Our observations unambiguously show that they are. The statistical association of galaxies with faint X-ray sources (in the form of X-ray fluctuations) has also

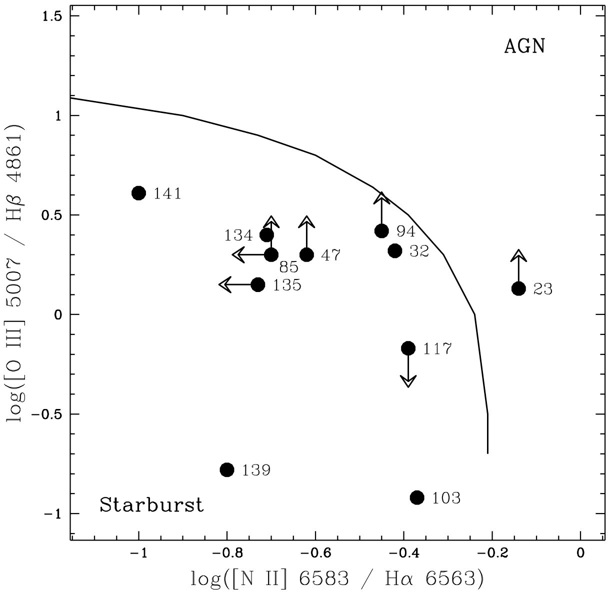

Figure 15. $[OIII]5007/H_\beta$ vs $[NII6583]/H_\alpha$ line ratio plot for all NELGs for which we have optical spectra within our 15 arcmin full survey area. Thus we include sources 139 and 141 which are below the flux limit of our complete survey. We also include the NELG which contributes part of the X-ray emission in source 23. Not all NELGs for which we have optical spectra are plotted as, in some cases, some of the spectral lines are not covered by our spectra. The solid line is the dividing line between AGN and HII region galaxies from Veilleux and Osterbrock (1987)

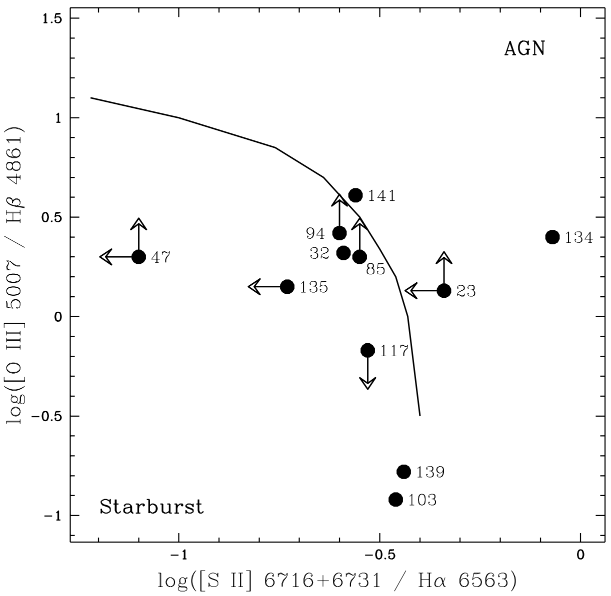

Figure 16. $[OIII]5007/H_\beta$ vs $[SII6716]/H_\alpha$ line ratio plot for the same sample as in figure 15.

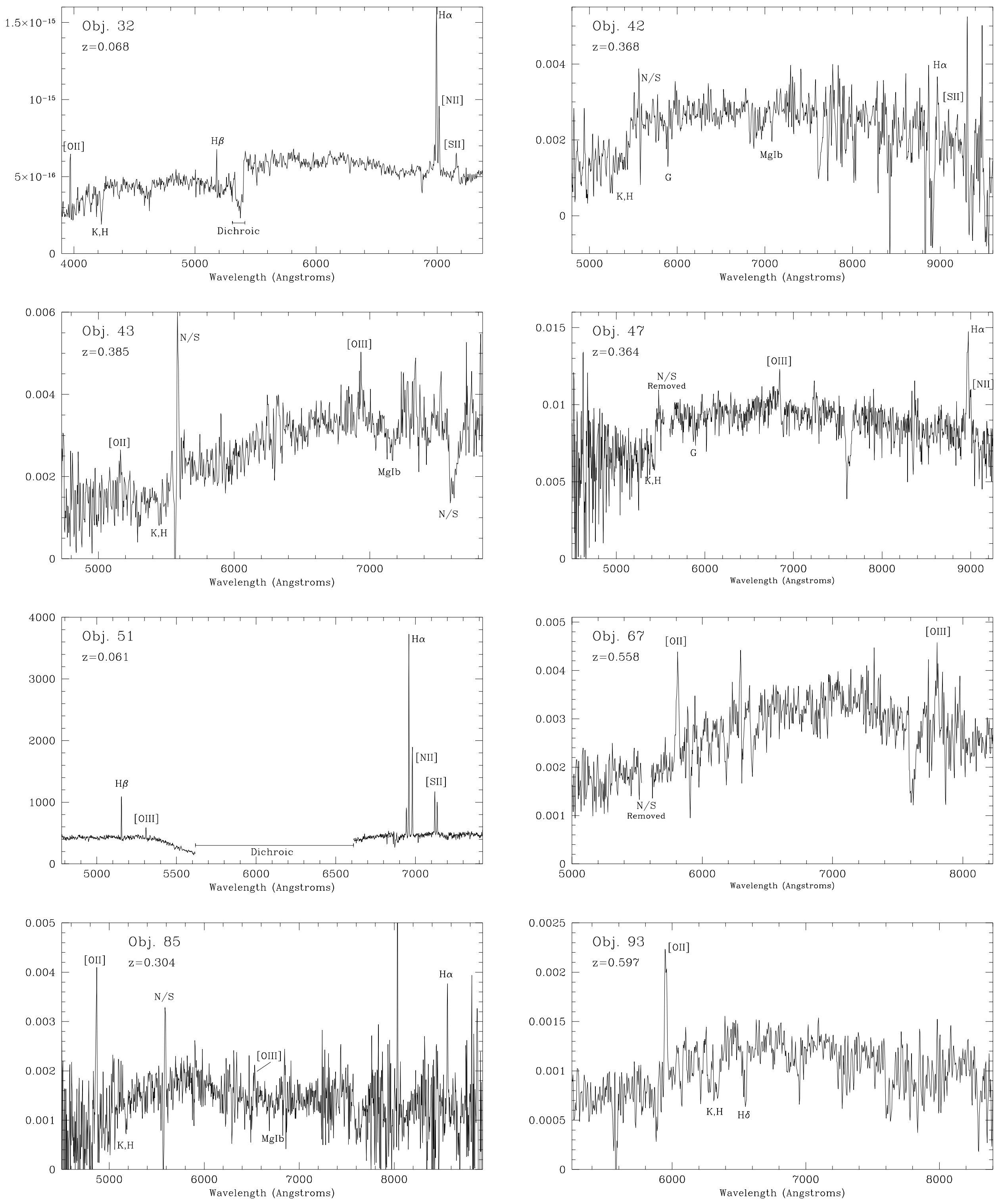

Figure 12. NELG optical spectra. With the exception of object 51 the spectra have been flux calibrated but the flux scales are arbitrary. The high resolution spectrum of object 51 was taken on a different observing run to all the other (low resolution) NELG spectra.

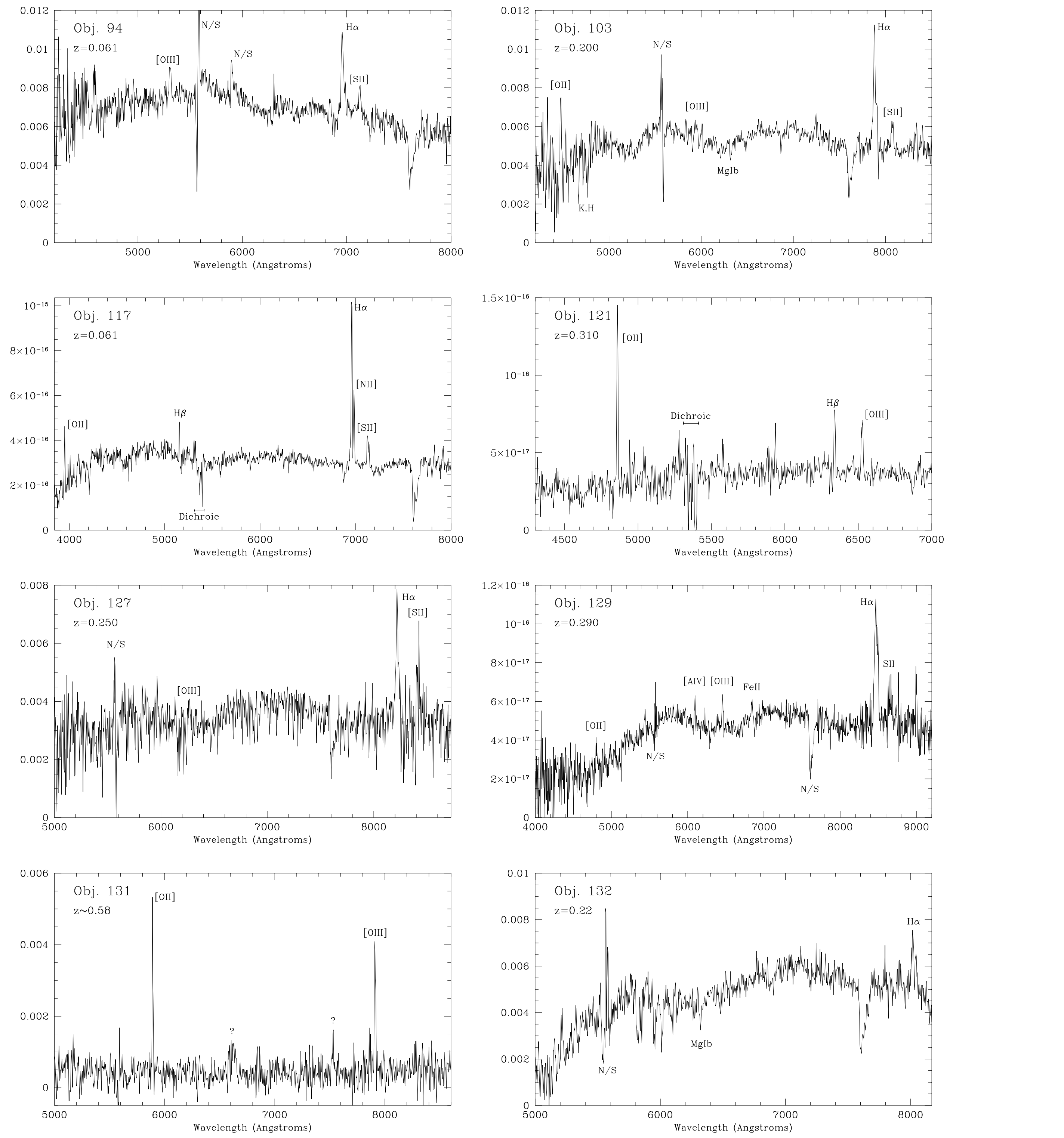

Figure 13. NELG optical spectra.

been reported previously. Lahav *et al.* (1993) find an association between GINGA X-ray fluctuations and UGC galaxies (of unknown spectral type) and, of particular relevance to the present work, Roche *et al.* (1995) find a 5σ correlation between galaxies of R<23 and fluctuations in a 50ksec ROSAT PSPC observation. However optical spectra are generally not available for the galaxies in the Lahav *et al.* and Roche *et al.* correlations and so their nature was unknown. Our observations indicate that those galaxies probably in-

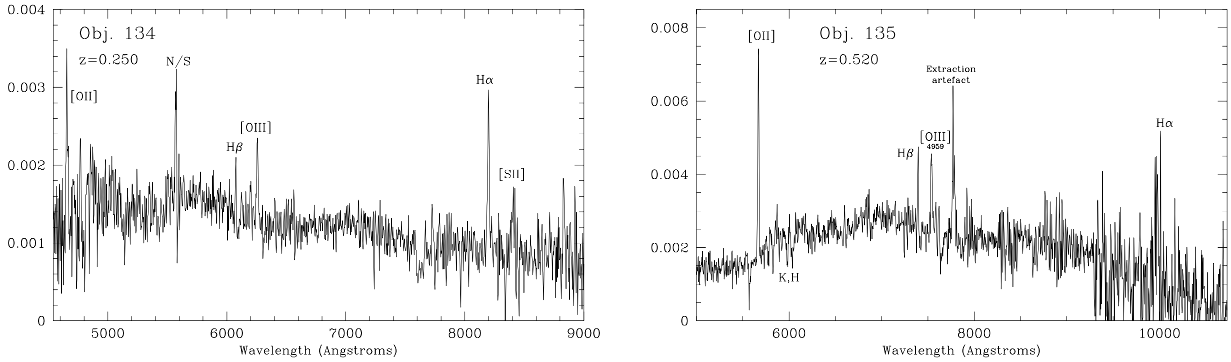

Figure 14. NELG OPTICAL SPECTRA. Note that in object 135 the [OIII] line is 4959, not 5007 which is obscured by a night sky feature. Also note the nearby extraction artefact. This artefact is not visible on another spectrum of this object which confirms [OII]3727, H_β and [OIII]4959 but does not cover H_α. The artefact arises because the object lies right on the edge of the slit.

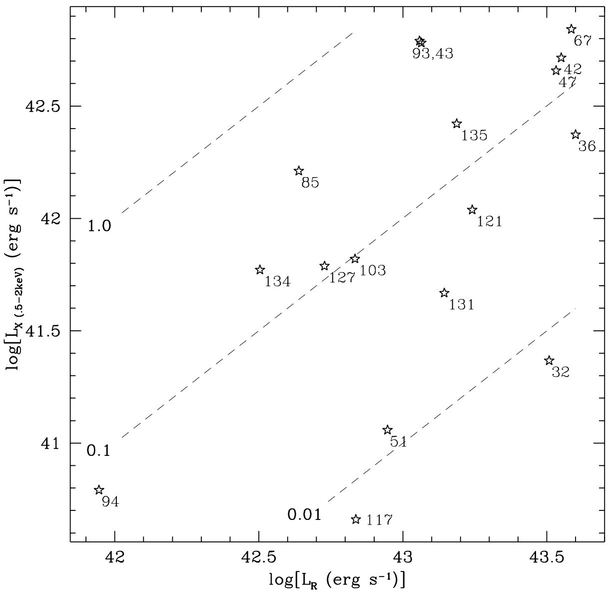

Figure 17. The rest frame X-ray and optical luminosities for the NELGs in our complete sample. L_X is the integrated flux from 0.5-2keV and L_R is the R band luminosity integrated over a 1000A band. $H_0 = 50, q_0 = 0.5$, $\alpha_{opt} = 1$ and $\alpha_X = 0.7$. The dashed lines are lines of constant X-ray/optical ratio. On average we expect AGN to have ratios near 1 and starburst galaxies to have ratios around 0.001. The majority of our NELGs lie somewhere inbetween indicating a possible mixture of X-ray emission mechanisms.

cluded a mixture of NELGs and the absorption line galaxies such as we find to be associated with groups and clusters.

8 COMPARISON OF THE NELGS WITH OTHER FAINT GALAXY POPULATIONS

Above we have discussed the likely nature of the NELGs. We see that they are generally of low ionisation but that some true AGN contribution, as well as a starburst contribution to the X-ray and optical emission, is likely in at least some NELGs. We have preliminary indications that the NELGs may be related to the faint radio galaxy population, and they are certainly related to starburst galaxies which are already well known to be moderately luminous X-ray sources (eg Griffiths and Padovani 1990; Rephaeli *et al.* 1991; Fruscione and Griffiths 1991; Moran, Halpern and Helfand 1994). However we note that the X-ray luminosities of the NELGs (3×10^{41} to 5×10^{42} ergs s^{-1}) are all well above the X-ray luminosities of typical starburst galaxies (maximum detected luminosity $\sim 2\times10^{41}$ ergs s^{-1}; Griffiths and Padovani 1990; Read and Ponman 1997). Thus either the NELGs are extreme examples of starburst galaxies or they contain another X-ray emission source, eg an AGN. If they are starbursts, then their implied far infrared luminosities should be detectable in deep ISO observations. There has been much speculation as to the likely contribution of starburst galaxies to the XRB but uncertainty in their evolution and in extrapolating to faint flux levels has prevented any reliable conclusions from being reached. We note that the NELGs are predominantly blue, and faint, and so we may speculate about their relationship to the faint blue galaxy population (eg Colless *et al.* 1990). However we note that, based on their angular correlation function, the faint blue galaxies have likely redshifts of 0.2-0.3 (Landy *et al.* 1996), a little lower than that of the NELGs. For that assumed redshift range, the faint blue galaxies have absolute magnitudes ~ 3 magnitudes fainter than the NELGs.

The obvious question therefore arises as to whether the various faint galaxy populations are really different in any way or merely different manifestations of broadly the same basic phenomenon. It is therefore interesting to compare our NELGs with the field galaxy population in a similar redshift range. Tresse et al (1996) have examined the spectra of 138 galaxies selected from an I-band magnitude limited sample ($17.5 \leq I \leq 22.5$) out to redshift 0.3. As their sample selects galaxies on the basis of their old stellar population it avoids bias towards starburst galaxies which dominate B-band or IRAS selected samples. However they still find that 85% of their sample display at least narrow line H_α in emission and 53% display, in addition, several forbidden emission lines; 17% of their galaxies display spectra consistent with Seyfert 2 galaxies. Only 15% display pure absorption line spectra.

The Tresse *et al.* sample shows a very similar distribution of emission line spectra to our NELGs and their emission line galaxies have a very similar distribution to our NELGs in the standard line ratio plots (Veilleux and Osterbrock 1987), straddling the boundary between AGN (Seyfert II) and HII region spectra. The distribution of [OII]3727 equivalent widths is very similar in our NELGs and in the Tresse *et al.* sample.

The average absolute magnitude of Tresse et al's emission line galaxies, $M_B = -18.4$, is less luminous than that of our NELGs (M_R -20 to -23) by around 3 magnitudes, but is similar to that estimated for the faint blue galaxies by Landy *et al.* Our NELGs may therefore just represent the more luminous examples of the emission line field galaxies. If the optically less luminous, but more numerous, emission line field galaxies produce similarly lower luminosity X-ray emission, then we may reasonably expect that the contribution of NELGs to the XRB will continue to rise at lower X-ray fluxes, supporting the extrapolations made in Section 6.

The Tresse *et al.* sample is selected up to redshift 0.3, whereas our NELGs reach redshift 0.6 thus the possibility of evolutionary differences between the two samples exists. Similarly, in the very local universe Huchra and Burgh (1992) find very few active galaxies indicating possible evolution in the activity of field galaxies between redshift 0 and 0.3. However, as discussed by Tresse *et al.* , the fraction of field galaxies which are active which is given by Huchra and Burgh (2%) should be treated cautiously and is probably an underestimate of the overall number of emission line galaxies (including galaxies other than Seyferts). Evolutionary uncertainties therefore prevent detailed extrapolation of the contribution of NELGs to the XRB at very faint fluxes, however we do note that Page *et al.* (1997b) find no strong evidence for evolution in the NELG populations found in the present survey and in the RIXOS survey and so the simple extrapolations given in Section 6 may not be too far wrong.

Thus we conclude that a substantial fraction of the XRB is contributed by field galaxies. The IRAS galaxies, and sub-mJy radio sources, are most likely simply the starburst-dominated fraction of these same emission line field galaxies.

9 CONCLUSION

In the deepest optically identified X-ray survey so far made, we have resolved approximately half of the X-ray background at 1 keV. The identifications are spectroscopically 85% complete to 2×10^{-15} erg cm^{-2} s^{-1} (0.5 -2.0 keV). At brighter fluxes ($\geq 10^{-14}$ erg cm^{-2} s^{-1}) we confirm the results of previous less deep X-ray surveys with 84% of our sources being QSOs. However at the faint flux limit the survey is dominated by a population of galaxies, mainly with narrow emission lines (NELGs). Whereas the QSO differential source count slope below 10^{-14} erg cm^{-2} s^{-1} is $\sim$-1.4, severely sub-Euclidean, the differential NELG slope is close to Euclidean (~ -2.4). To the survey limit QSOs still contribute the largest identified fraction of the XRB, >31% as opposed to 8% for NELGs and 10% for clusters. We note that a small number of the fainter NELGs may be misidentifications and that some of the unidentified sources are almost certainly faint QSOs, although some are also likely to be either NELGs or clusters. However as we are unable to correct our observed contributions to the XRB until these sources are properly identified, we simply note that all of our contributions are observed values. However if the observed differential source counts can be reliably extrapolated to fainter fluxes, clusters will contribute almost nothing more to the XRB and QSOs will contribute only a small amount more. On the other hand the NELG contribution to the XRB will double by a flux limit a factor 4 below the present survey.

The NELGs observed so far lie in the redshift range 0.1-0.6, as one might expect given an identification limit of R=23. It is not yet clear whether there is any astrophysical significance to the maximum observed redshift. The NELGs have generally blue colours, and have optical spectra similar to that of the active field galaxy population at a similar redshift. Some NELGs are definitely large spirals but the possibility that some are ellipticals cannot be ruled out on the basis of the present analysis. Many of the NELGs are in disturbed or interacting systems. The NELGs, both as a sample and individually, appear to be a mixture of starburst galaxies and true AGN. By comparison with the field galaxy surveys of Tresse *et al.* , the simplest interpretation of our results is that the NELGs which we detect are simply the more luminous members of the normal field galaxy population.

The average NELG X-ray spectrum is harder than that of the QSOs, and similar to that of the remaining unresolved cosmic soft X-ray background (XRB). NELGs should therefore be a major contributor to the XRB at higher energies although without a detailed understanding of the NELG X-ray emission mechanism it is not possible to say up to which energies one might reasonably expect them to contribute. However their fluxes at higher energies will still be low ($< 10^{-14}$ erg cm^{-2} s^{-1}, 2-10 keV) and so they may not show up in large numbers in ASCA surveys but should be prominent in surveys with XMM and AXAF.

We also find that a small number of groups or clusters of galaxies are identified as X-ray sources. So far we have not found any X-ray identifications with entirely isolated absorption line galaxies. All such galaxies appear to have at least a few faint companions. However the groups/clusters are generally not very rich. The number of groups found is in approximate agreement with a zero-evolution scenario for low luminosity clusters, unlike the situation for rich clusters in the same redshift range ($Z > 0.3$).

REFERENCES

Almaini, O., Shanks, T., Boyle, B.J., Griffiths, R.E., Roche, N., Stewart, G.C. and Georgantopoulos, I., 1996. MNRAS 282, 295.

Barcons, X., Branduardi-Raymont, G., Warwick, R.S., Fabian, A.C., Mason, K.O., McHardy, I.M. and Rowan-Robinson, M., 1994. MNRAS, 268, 833.

Benn, C.R., Rowan-Robinson, M., McMahon, R.G., Broadhurst, T.J. and Lawrence, A., 1993. MNRAS 263, 98.

Boller, Th, Meurs, E.J.A., Dennefeld, M., Fink, H., 1993. ApSS 205, 43.

Boyle, B.J., Griffiths, R.E., Shanks, T., Stewart, G.C. and Georgantopoulos, I. 1993. MNRAS, 260, 49.

Boyle, B.J., Jones, L.R. and Shanks, T., 1991. MNRAS, 251. 482.

Boyle, B.J., Shanks, T., Georgantopoulos, I., Stewart, G.C. & Griffiths, R.E., 1994. MNRAS, 271, 639.

Boyle, B.J., McMahon, R.G., Wilkes, B.J. and Elvis, M., 1995. MNRAS, 272, 462.

Branduardi-Raymont, G., et al., 1994. MNRAS, 270, 947.

Briel, U.G. *et al.* 1995. 'The ROSAT Users Handbook', MPE.

Cash, W., 1979. ApJ 228, 939.

Carballo, R., Warwick, R.S., Barcons, X., Ganzalez-Serrano, J.I., Barber, C.R., Martinez-Gonzalez, E., Perez-Fournon, I., Burgos, J., 1995. MNRAS, 277, 1312.

Castander, F.J. *et al.* 1995. Nature, 377, 39.

Colless, M.M., Ellis, R.S., Taylor, K. and Hook, R.N., 1990. MNRAS, 244, 408.

Collins, C.A., Burke, D.J., Romer, A.K., Sharples, R.M., and Nichol, R.C., 1997. ApJ Lett, submitted.

Condon, J.J., 1992. ARAA, 30, 575.

Done, C, Madejski, G.M. and Smith, D.A., 1997. ApJ Lett (in press).

David, L.P., Jones,C., Forman, W., 1992. ApJ 388, 82.

Ebeling, H., Edge, A.C., Fabian, A.C., Allen, S.W., Crawford, C.S. & Bohringer, H. 1997, ApJ, submitted.

Edge, A.C., Stewart, G.C., Fabian, A.C. and Arnaud, K.A., 1990. MNRAS 245, 559.

Elvis, M., Maccacaro, T., Wilson, A.S., Ward, M.J., Penston, M.V., Fosbury, R.A.E, and Perola, G.C., 1978. MNRAS, 183, 129.

Fabian, A.C. and Barcons, X., 1992. ARAA 30, 429.

Fabbiano, G., 1989. ARAA, 27, 87.

Fabbiano, G. and Trinchieri, G., 1985. ApJ 296, 430.

Ferland, G. and Netzer, H., 1983. ApJ 264, 105.

Fruscione, A. and Griffiths, R.E., 1991. ApJ 380, L13.

Gendreau, K.C. etal. 1995, PASJ., 47, L5.

Gioia, I.M., Maccacaro, T., Schild, R.E., Wolter, A., Stocke, J.T., Morris, S.L. & Henry, J.P. 1990a ApJS 72, 567.

Gioia, I.M., Henry, J.P., Maccacaro, T., Morris, S.L., Stocke, J.T. and Wolter, A., 1990b. ApJ 356, 35.

Griffiths, R.E. and Padovani, 1990 ApJ 360, 483.

Griffiths, R.E., Della Ceca, R., Georgantopoulos, I., Boyle, B.J., Stewart, G.C., Shanks, T. and Fruscione, A., 1996. MNRAS, 281, 71.

Hall, P.B., Osmer, P.S., Green, R.F., Porter, A.C. and Warren, S.J., 1996. ApJ 462, 614.

Hasinger, G., Burg,R., Giacconi, R., Hartner, G., Schmidt, M., Trumper, J., Zamorani, G. 1993, A&A 275, 1.

Henry, J.P., Gioia, I.M., Maccacaro, T., Morris, S.L., Stocke, J.T., Wolter, A. 1992, ApJ, 386, 408.

Huchra, J. and Burgh, R., 1992. ApJ 393, 90.

Jones, L.R., *et al.* 1995. Proc 35th Herstmonceux Conf, P339. ed Maddox, S.

Jones, L.R., M^{c}Hardy, I.M., Merrifield, M.R., Mason, K.O., Smith, P.J., Abraham, R.G., Branduardi-Raymont, G., Newsam, A.M., Dalton, G., Rowan-Robinson, M. and Luppino, G., 1997. MNRAS, in press.

Kennicutt, R.C., 1992. ApJ 388, 310.

Lahav, O., Fabian, A.C., Barcons, X., Boldt, E., Butcher, J., Carrera, F.J., Jahoda, K., Mitaji, T., Stewart, G.C. and Warwick, R.S., 1993. Nature, 364, 693.

Landy, S.D., Szalay, A.S. and Koo, D.C., 1996. ApJ 460, 94.

Leach, C.M., M^{c}Hardy, I.M. and Papadakis, I.E., 1995. MNRAS, 272, 221.

Maccacaro, T., Della Ceca, R., Gioia, I.M., Morris, S.L., Stocke, J.T., & Wolter, A. 1991 ApJ 374, 117.

Mather, J.C., et al. 1990. ApJ 354, L37.

M^{c}Hardy, I.M., Lawrence, A., Pye, J.P. and Pounds, K.A., 1981. MNRAS, 197, 893.

M^{c}Hardy, I.M, 1995. Spectrum, 6, 11.

Metcalfe, N., Shanks, T., Fong, R., and Jones, L.R., 1991. MNRAS 249, 498.

Metzger, M.R., Luppino, G.A. and Miyazaki, S., 1995. BAAS 187, 73.05.

Moorwood, A.F.M., 1996. Sp. Sc. Rev., 77, 303.

Moran, E.C., Halpern, J.P. and Helfand, D.J., 1994. ApJ 433, L65.

Narayan, R. and Yi, I., 1995. ApJ 452, 710.

Newsam, A.M., M^{c}Hardy, I.M., Jones, L.R., and Mason, K.O., 1997. MNRAS (in press).

Page, M.J., Mason, K.O., M^{c}Hardy, I.M., Jones, L.R. and Carrera, F.J., 1997a. MNRAS (submitted)

Page, M.J., Mason, K.O., M^{c}Hardy, I.M., Jones, L.R. and Carrera, F.J., 1997b. MNRAS (submitted)

Pearson, C., Rowan-Robinson, M.R., M^{c}Hardy, I.M., Jones, L.R., and Mason, K.O., 1997. MNRAS (submitted).

Read, A.M. and Ponman, T.J., 1997. MNRAS (submitted).

Rephaeli, Y., Gruber, D., Persic, M. and MacDonald, D., 1991. ApJ 380, L59.

Rephaeli, Y., Gruber, D., Persic, M., 1995. A&A 300, 91.

Roche, N., Shanks, T., Georgantopoulos, I., Stewart, G.C., Boyle, B.J. and Griffiths, R.E., 1995. MNRAS, 273, 15.

Romero-Colmenero, E., Branduardi-Raymont, G., Carrera, F.J., Jones, L.R., Mason, K.O., M^{c}Hardy, I.M. and Mittaz. J.P.D., 1996. MNRAS, 282, 94.

Scharf, C.A., Jones, L.R., Perlman, E., Ebeling, H., Wegner, G., Malkan, M., Horner, D. 1997. Proceedings of Texas Symposium, Chicago, Dec 1996, in press.

Schade, D., Crampton, D., Hammer, F., Le Fevre, O. and Lilly, S.J., 1996. MNRAS 278, 95.

Shanks, T., Georgantopoulos, I., Stewart, G.C., Pounds, K.A., Boyle, B.J. and Griffiths, R.E. 1991. Nature, 353, 315.

Stark, A.A., Gammie, C.F., Wilson, R.W., Bally, J., Linke, R.A., Heiles, C. and Hurwitz, M., 1992. ApJS, 79, 77.

Stocke, J.T., Morris, S.L., Gioia, I.M., Maccacaro, T., Schild, R., Wolter, A., Fleming, T.A., Henry, J.P. 1991 ApJS 76, 813.

Tresse, L., Rola, C., Hammer, F. and Stasinska, G., Le Fevre, O., Lilly, S.J. and Crampton, D., 1996. MNRAS, 281, 847.

Turner, M.J.L., *et al.* , 1990. MNRAS, 244, 310.

Turner, T.J., Urry, C.M. and Mushotzky, R.F., 1993. ApJ 418, 653.

Veilleux, S. and Osterbrock, D.E., 1987. ApJS 63, 295-310.

Zitelli,V., Mignoli, M., Zamorani, G., Marano, B. and Boyle, B.J., 1992. MNRAS 256, 349.

ACKNOWLEDGEMENTS

We thank the following observatories and their staff for support of this project: the Canada-France-Hawaii Telescope, the UK William Herschel Telescope, the Nordic Optical Telescope, the University of Hawaii 88 inch Telescope the Mitchigan-Dartmouth-MIT Telescope and the Very Large Array Radio Telescope. We thank Craig Collins for careful analysis of the extended X-ray sources. This work was supported by grants to a number of authors from the UK Science and Engineering Research Council and Particle Physics and Astronomy Research Council. KOM acknowledges support from the Royal Society. FJC acknowledges partial financial support from the DGES under project PB95-0122.